

Abundances and search for vertical stratification in the atmospheres of four HgMn stars

M. Thiam^{1*}, F. LeBlanc¹, V. Khalack¹, G.A. Wade²

¹*Département de Physique et d'Astronomie, Université de Moncton, Moncton, N.-B., E1A 3E9, Canada*

²*Department of Physics, Royal Military College of Canada, PO Box 17000 stn 'FORCES', Kingston, Ontario, K7K 7B4, Canada*

Accepted . Received ; in original form

ABSTRACT

Using high resolution, high-S/N archival UVES spectra, we have performed a detailed spectroscopic analysis of 4 chemically peculiar HgMn stars (HD 71066, HD 175640, HD 178065 and HD 221507). Using spectrum synthesis, mean photospheric chemical abundances are derived for 22 ions of 16 elements. We find good agreement between our derived abundances and those published previously by other authors. For the 5 elements that present a sufficient number of suitable lines, we have attempted to detect vertical chemical stratification by analyzing the dependence of derived abundance as a function of optical depth. For most elements and most stars we find no evidence of chemical stratification with typical 3σ upper limits of $\Delta \log N_{\text{elem}}/N_{\text{tot}} \sim 0.1 - 0.2$ dex per unit optical depth. However, for Mn in the atmosphere of HD 178065 we find convincing evidence of stratification. Modeling of the line profiles using a two-step model for the abundance of Mn yields a local abundance varying approximately linearly by ~ 0.7 dex through the optical depth range $\log \tau_{5000} = -3.6$ to -2.8 .

Key words: stars: abundances - stars: atmospheres - stars: chemically peculiar - stars: individual: HD 71066 (κ^2 Vel), HD 175640 (HR 7143), HD 178065 (HR 7245), HD 221507 (β Scl)

1 INTRODUCTION

Chemically peculiar (CP) stars are A- and B-type stars exhibiting peculiar chemical abundances and slow rotation. With effective temperatures ranging between 10 000 K and 15 000 K, the late B-type HgMn stars belong to the third group of CP stars defined by Preston (1974). They are characterized spectroscopically by large overabundances of Hg (possibly up to 6 dex; Heacox 1979, Cowley et al. 2006) and Mn (possibly up to 3 dex; Aller 1970). Overabundances greater than 2 dex of Be, Ga, Y, Pt, Bi, Xe, Eu, Gd, W and Pb are frequently observed in these stars, while He, N, Mg, Al, Ni and Zn often are underabundant by more than 0.5 dex (Takada-Hidai 1991). The elements C, O, Si, S, Ca, V, Cr and Fe usually show only modest peculiarities, with abundances within 0.5 dex of their solar abundances (classified as "normal type" elements by Takada-Hidai 1991).

HgMn stars rotate slowly in comparison to "normal" late-B stars, with $v \sin i < 100$ km s⁻¹. Their average rotation velocity is estimated to be 29 km s⁻¹ (Abt et al. 1972). These stars present a high rate of binarity: Gerbaldi et al. (1985) estimate that 51% are members of binary systems. Most of these binary systems have relatively small separations, with 41% belonging to SB1 systems, while 59% belong to SB2 systems. Some authors (Mathys & Hubrig 1995; Hubrig et al. 1999; Hubrig & Castelli 2001) have re-

ported the presence of a weak magnetic fields in the atmospheres of some HgMn stars. However, attempts to confirm these claims for other HgMn stars have been unsuccessful (Landstreet 1982; Shorlin et al. 2002; Wade et al. 2006). In light of the lack of convincing evidence, we assume for the purposes of this study that HgMn stars are non-magnetic objects. Because of their high effective temperatures, the HgMn stars should not host hydrogen convective zones in their envelopes, and their low He abundances may reduce the importance of He convection zones as well. Indeed, Adelman (1994) showed that HgMn stars have small microturbulent velocities. Atmospheric velocity fields are estimated to be less than 1 km s⁻¹ for stars with T_{eff} ranging between 10 200 K and 12 000 K (Landstreet 1998).

The slow rotation and weak microturbulence of HgMn stars suggest that their atmospheres should be hydrodynamically stable. Atomic diffusion (Michaud 1970), resulting from the competition between local gravitational settling and radiative acceleration, may therefore play an important role in determining the chemical properties of their outer layers. A natural consequence of diffusion is the presence of non-uniform vertical distributions of chemical abundances (chemical stratification). Detecting and characterizing such stratification is the primary goal of this study.

Several investigations aimed at the detection of chemical stratification in atmospheres of HgMn stars were undertaken in the past. Savanov & Hubrig (2003) reported stratification of Cr in a sample of 10 HgMn stars. Their method involved the derivation of the

* E-mail: emt9755@umoncton.ca

Table 1. Journal of observations and stellar parameters of studied stars.

HD	Other name	HJD	Program ID	Binarity	T_{eff} (K)	$\log g$ (cgs)	V_r (km s ⁻¹)	$v \sin i$ (km s ⁻¹)	Reference
71066	κ^2 Vel	2453098.50	60.A-9022		12 010	3.95	+16.8	2.0	Hubrig et al. (1999)
175640	HR 7143	2452074.89	67.D-0579	SB1	11 958	3.95	-34.2	2.0	Hubrig et al. (1999)
178065	HR 7245	2452074.92	67.D-0579	SB1	12 193	3.54	-34.8	1.5	Hubrig et al. (1999)
221507	β Scl	2452435.94	266.D-5655		12 476	4.13	-24.1	25.0	Dolk et al. (2003)

abundance of Cr from 8 lines of Cr II multiplet 30 located in the Stark-broadened wings of the H β line. According to these authors, the average chromium abundance from 9 stars of their sample, increases toward the core of H β , and therefore presumably toward the upper atmosphere by 0.34 ± 0.12 dex. The difference of 0.2 dex in the average abundances between Cr I and Cr II in the HgMn star HD 175640, obtained by Castelli & Hubrig (2004), is interpreted by these authors as a confirmation of Cr stratification found by Savanov & Hubrig (2003). An increase of Mn toward the upper atmosphere of HgMn stars was reported by Alecian (1982) and Sigut (2001). Evidence of the stratification of Ga has also been published by Lanz et al. (1993).

Meanwhile, Dubaj et al. (2004) modeled Fe lines in the spectrum of the HgMn star HD 143807A shortward and longward of the Balmer jump. They found no conclusive evidence of Fe stratification. This suggests that if stratification of these elements is present in the atmospheres of HgMn stars, it is relatively weak (in comparison to that frequently observed in magnetic Ap stars, for example - e.g. Ryabchikova et al. 2005).

Additional evidence for the presence of chemical stratification in HgMn stars has also been published. Sigut et al. (2000) signaled the discovery of Mn II, P II and Hg II emission lines in the spectrum of the HgMn star 46 Aql. Sigut (2001) interpreted these emission lines as the result of interlocked non-Local Thermodynamic Equilibrium (NLTE) processes in the presence of chemical stratification. Wahlgren & Hubrig (2000) also identified several emission lines of other elements, mostly Cr II and Mn II, in the spectra of some HgMn stars. They postulated that the emissions of the aforementioned elements in the red spectral region arise from a selective excitation process involving Ly α photon energies.

Very recently, Khalack et al. (2007 and 2008) have detected stratification of several elements including Fe in Blue Horizontal Branch (BHB) stars, evolved objects with effective temperatures similar to those of HgMn stars. These authors found that the iron abundance increases toward the lower atmosphere in three BHB stars. They also reported nitrogen and sulfur stratification in the hot BHB star HD 135485. In this star, the abundances of those elements increase toward the upper atmosphere. The method used to detect vertical stratification in BHB stars in the aforementioned papers is applied here to HgMn stars.

The aim of this paper is to search for vertical stratification of elements in the atmospheres of HgMn stars. Our approach is to model a large number of absorption lines of many different elements, and to examine the variation of the derived abundances as a function of optical depth. The mean abundances of the various elements analyzed will also be obtained.

2 OBSERVATIONS AND SPECTRAL REDUCTION

Spectra of the HgMn stars HD 71066 (κ^2 Vel), HD 175640 (HR 7143), HD 178065 (HR 7245) and HD 221507 (β Scl) were obtained from the ESO Science Archive¹. The Heliocentric Julian Date and program ID of these stars are summarized in Table 1. The spectra were obtained with the VLT UV-Visual Echelle Spectrograph (UVES) on the UT2 unit telescope. This instrument covers a wide spectral region from $\lambda = 3040 \text{ \AA}$ to $10\,000 \text{ \AA}$. The slit widths for the two arms of UVES were $0.4''$ for the blue and $0.3''$ for the red. The resultant resolving power is approximately $\lambda/\Delta\lambda = 80\,000$ in the blue and $110\,000$ in the red. The recorded spectra exhibit gaps which are located between $5730 - 5840 \text{ \AA}$ and $8510 - 8660 \text{ \AA}$.

Spectral reduction was performed using the UVES pipeline Data Reduction Software (version 2.2.0) for the 346 (304 - 388 nm) and 437 (373 - 499 nm) settings. Each order of these spectra was normalized using the IRAF “continuum” procedure. The signal-to-noise ratio after normalization ranges between $S/N = 200$ and 600 . For the 580 (476 - 684 nm) and 860 (660 - 1040 nm) settings, we used a software provided by V. Tsymbal (private communication) for spectral reduction and normalization, because it works faster and has convenient interface.

Before adopting Tsymbal’s code, we applied it to reduce the 580 settings for two stars of our sample. The same procedure was also performed using the UVES pipeline. A comparison of the resulting reduced spectra yields excellent agreement. After spectral normalization, observed and synthetic line profiles were compared to determine the radial velocities of our sample of stars. The radial velocity obtained for each star is reported in col. 8 of Table 1.

3 SPECTRUM SYNTHESIS

In our analysis, we have adopted the stellar atmosphere parameters derived for the investigated stars by Hubrig et al. (1999) and Dolk et al. (2003). The adopted atmospheric and spectroscopic parameters, including the effective temperature, surface gravity and projected rotational velocity, are reported in Table 1. The atmosphere models used for spectrum synthesis are computed with ATLAS9 (Kurucz 1993). They are calculated with a solar metallicity and a microturbulent velocity $\xi = 2.0 \text{ km s}^{-1}$. For atomic data, we used primarily the Vienna Atomic Line Database² (VALD) (Martin et al. 1988; Kurucz 1993 and 1994; Kupka et al. 1999; Ryabchikova et al. 1999). We also extracted some phosphorus and mercury atomic data from the National Institute of Standards and Technology³ (NIST) (Martin et al. 1985; Ralchenko et al. 2007). The NIST database was used because VALD does not provide a

¹ http://archive.eso.org/eso/eso_archive_main.html

² <http://ams.astro.univie.ac.at/vald>

³ http://physics.nist.gov/PhysRefData/ASD/lines_form.html

large number of P and Hg atomic data. Meanwhile, titanium atomic data from Pickering et al. (2001) have been used to compare the derived abundances from different sources. The lines and associated atomic data used in our analysis are summarized in Table 9 (online material).

To determine elemental abundances and to characterize the optical depth of line formation, we used the ZEE MAN2 LTE spectrum synthesis code (Landstreet 1988; Wade et al. 2001a). Although developed for spectrum synthesis of magnetic stars, this code is also able to reproduce stellar spectra in the non-magnetic case, including the effects of non-solar and vertically-stratified abundances.

As shown by Adelman (1994) and Landstreet (1998), and implicitly confirmed in the study of Dolk et al. (2003), HgMn stars have small microturbulent velocities. In this study, line profiles were synthesized assuming $\xi = 0 \text{ km s}^{-1}$, an assumption that will be verified *a posteriori* in Sect. 4. Since we desire high precision results, we carefully pre-selected lines to avoid blends and misidentifications. We also only selected lines located within spectral orders longward of the Balmer jump, in the 437 and 580 settings, for which $S/N \geq 300$. For our spectral analysis, each line profile of a particular species is fitted independently, while assuming a vertically-uniform abundance of the element in the atmosphere.

Hyperfine and isotopic splitting are respectively important for Mn (Jomaron et al. 1999) and Hg (White et al. 1976; Smith 1997; Dolk et al. 2003) line profiles synthesis in HgMn stars. When modeling these lines, we include the data of Mn hyperfine structure (hfs) and Hg isotopic splitting, when they are available. The data for Mn hyperfine structure are taken from Holt et al. (1999), while those of the Hg isotopic splitting are from Dolk et al. (2003). These data are summarized respectively in Table 6 and Table 7 (online material). Otherwise, lines are synthesized without this data. This leads us to ignore lines with a large reduced χ^2 , related to the difference between the observed and synthesized lines. The same procedure is used for all analyzed elements. Fig. 1 shows the Mn II λ 4206 line with the hfs data of the line taken into account and without it. These results show that the synthetic Mn II λ 4206 line is better fitted when the hfs data is taken into account, except for the fast rotating star HD 221507. For this star, no significant difference is observed between the fits with and without hfs data. Nevertheless, the abundance obtained from the hfs data of this line for HD 221507, is closer to the mean abundance of Mn measured in the atmosphere of this star. The consideration of the isotopic composition of Hg II λ 3984 agrees with observed lines (see Fig. 2). Both the core and wings of this line are better fitted by taking into account the isotopic composition. The isotopic mixture of mercury for the peculiar Hg II λ 3984 line is presented in Table 8 (online material).

During the spectral synthesis, the continuous opacities for H I, H⁻ and He I bound-free (b-f) and free-free (f-f) transitions are computed. Photons scattering by free electrons and H I atoms are also taken into account in the opacity calculations, as well as line broadening due to the natural, Doppler and pressure broadenings. For more details, see Wade et al. (2001a). To fit a line, we simultaneously determine the element's abundance $\log(N_{ion}/N_{tot})$, the stellar radial velocity V_r and projected rotational velocity $v \sin i$ by minimizing the deviation between the simulated and observed line profiles. The optical depth of formation of the line is defined as the continuum optical depth τ_{5000} where the monochromatic optical depth of the line centre is equal to unity (Khalack et al. 2007 and 2008).

Two stars studied here are SB1 and the others are non-binary

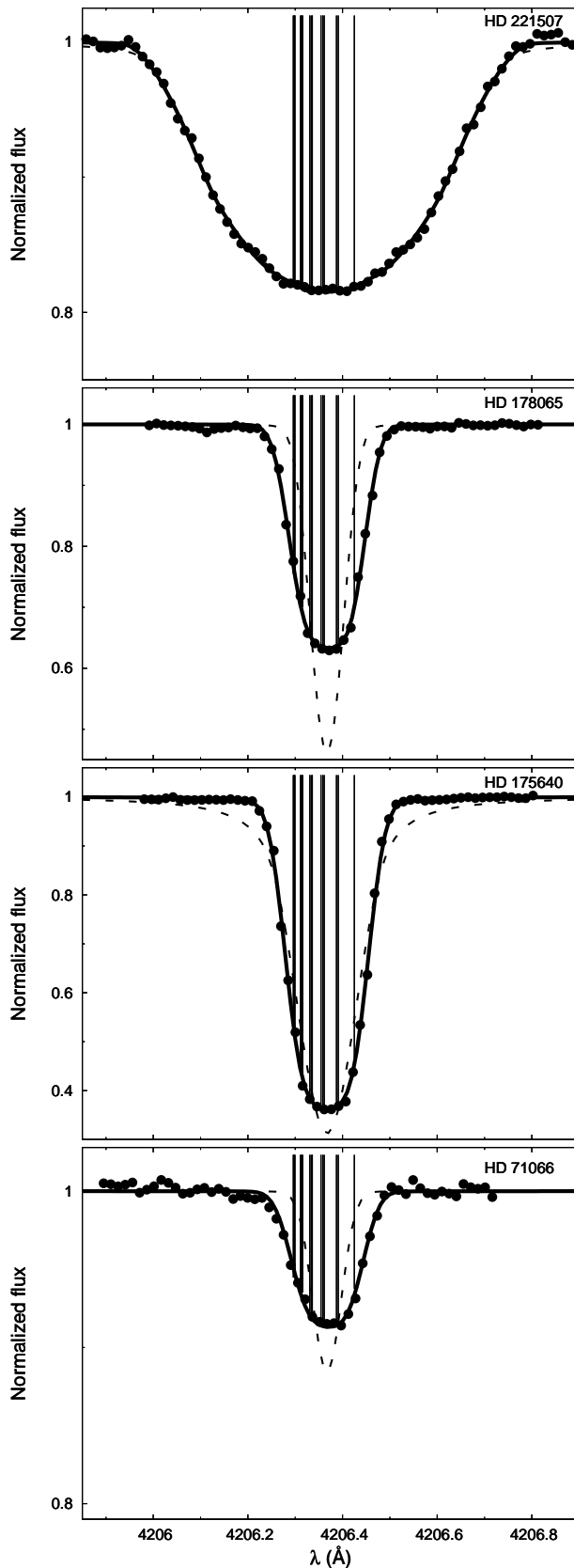


Figure 1. The Mn II λ 4206 line observed (dots) for HD 71066, HD 175640, HD 178065 and HD 221507. This line is fitted by assuming a single-line component (dashed curve) and the hfs data (solid curve). The vertical lines represent the hfs line positions.

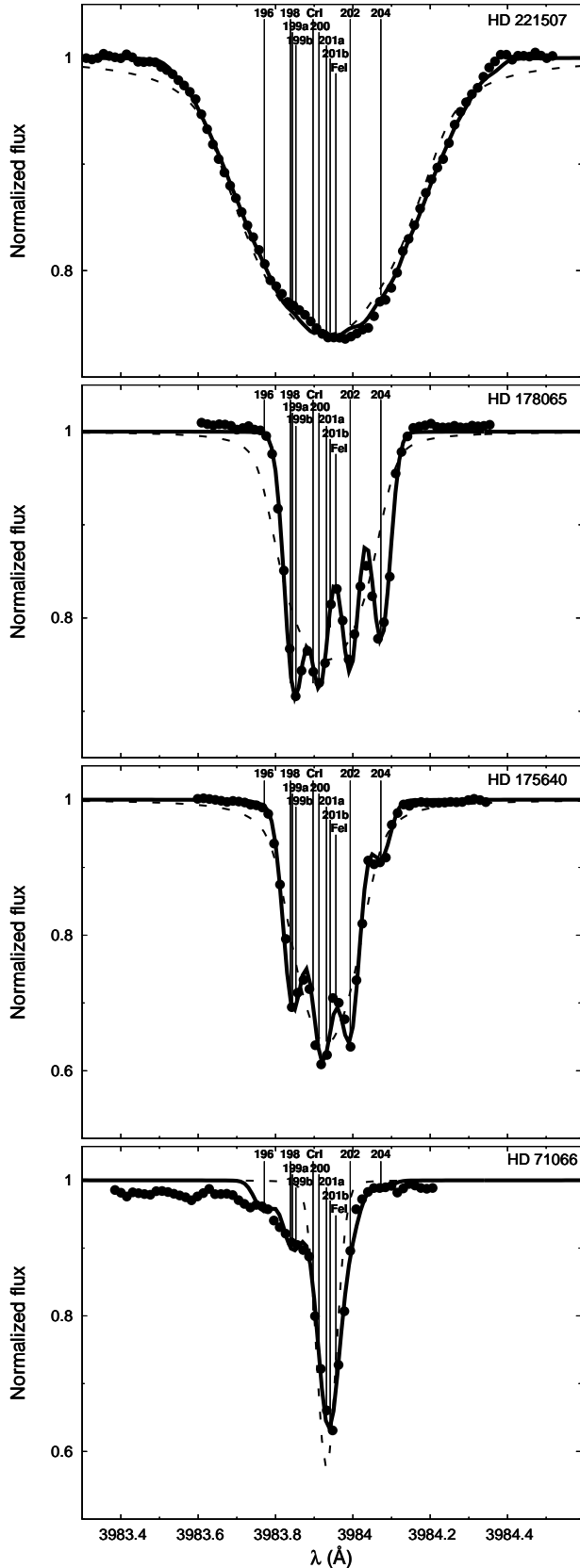


Figure 2. Same description as in Fig. 1, but for the observed Hg II λ 3984 line (dots), fitted by assuming a single-line component (dashed curve) and the isotopic composition (solid curve). The vertical lines represent the lines of the various isotopes and blends.

Table 2. Effective temperature, luminosity, mass and age of studied stars. The approximate errors in effective temperatures and luminosities are respectively $\pm 5\%$ and ± 0.1 dex.

HD	T_{eff} (K)	$\log(L/L_{\odot})$ (dex)	M/M_{\odot}	$\log t$
71066	12 010	2.05	3.09	8.11
175640	11 958	2.08	3.21	8.16
178065	12 193	2.26	3.31	8.21
221507	12 476	1.88	3.07	6.09

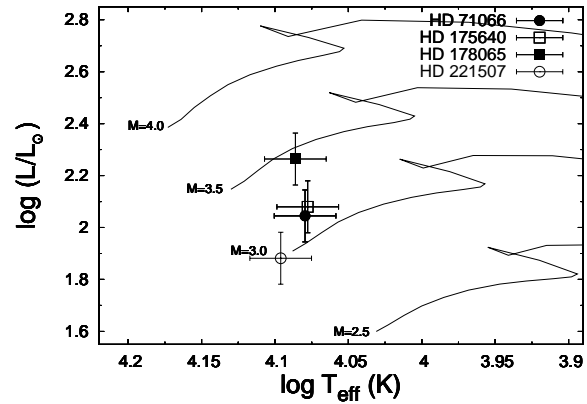


Figure 3. The positions of HD 71066 (filled circle), HD 175640 (empty square), HD 178065 (filled square) and HD 221507 (empty circle) in the Hertzsprung-Russell diagram assuming that their temperatures and luminosities are respectively known within $\pm 5\%$ and ± 0.1 dex. These positions are determined using the standard evolution track $Z=0.02$ (Schaller et al. 1992).

(see Table 1). Since the contribution of the companion star for SB1 systems is not observed in the spectra, in this paper the SB1 stars are treated as single stars. The position in the Hertzsprung-Russell (HR) diagram of each star was determined photometrically. The effective temperature and surface gravity used are those from Table 1. The Johnson magnitude and Strömgren indices in the $ubvy$ photometric system are extracted from the General Catalogue of Photometric Data⁴. Stars' parallax values are extracted from Hipparcos catalogue⁵. The bolometric correction was calculated as in Balona (1994). The parameters such as $\log(L/L_{\odot})$, M/M_{\odot} and $\log t$ presented in Table 2, are determined using the evolutionary model calculations of Schaller et al. (1992) with $Z = 0.02$. The position of stars in the HR diagram ($\log(L/L_{\odot})$, $\log(T_{\text{eff}})$) is presented in Fig. 3. As shown in this figure, all stars studied here belong to the main sequence. HD 221507 is the youngest star, while the others appear to be somewhat older.

4 AVERAGE ABUNDANCES

The mean abundances $\log(N_{\text{ion}}/N_{\text{tot}})$ measured in the atmospheres of the HgMn stars HD 71066, HD 175640, HD 178065 and HD 221507 are reported in Table 3. Several error sources have to be taken into account. For example, Khan & Shulyak (2007) show

⁴ <http://obswww.unige.ch/gcpd/gcpd.html>.

⁵ <http://cdscwww.hia.nrc.ca/astrocat/hipparcos/>

Table 3. Mean abundances $\log(N_{ion}/N_{tot})$ of chemical species measured in the atmospheres of HD 71066, HD 175640, HD 178065 and HD 221507.

Ion	HD 71066	HD 175640	HD 178065	HD 221507	Sun		
					[A]	[B]	[C]
He I	-2.30 ± 0.40	-1.65 ± 0.13	-1.78 ± 0.12	-1.93 ± 0.14	-1.05	-1.07 ± 0.01	0.02
C II	-3.89 ± 0.10	$-3.86 \pm 0.10^*$	$-3.78 \pm 0.05^*$	$-3.92 \pm 0.05^*$	-3.48	-3.61 ± 0.05	0.13
O I	-3.61 ± 0.14	-3.24 ± 0.04	-3.33 ± 0.15	$-3.11 \pm 0.09^*$	-3.11	-3.34 ± 0.05	0.23
Mg I	...	$-4.78 \pm 0.06^*$	$-4.86 \pm 0.04^*$	$-4.40 \pm 0.10^*$	-4.46	-4.47 ± 0.09	0.01
Mg II	-5.46 ± 0.01	-4.86 ± 0.01	-5.02 ± 0.03	-4.73 ± 0.18	-4.46	-4.47 ± 0.09	0.01
Si II	-4.58 ± 0.07	-4.69 ± 0.03	-4.58 ± 0.12	-4.53 ± 0.06	-4.49	-4.49 ± 0.04	0.00
P II	-4.87 ± 0.22	-6.37 ± 0.15	-5.26 ± 0.15	-5.42 ± 0.38	-6.59	-6.64 ± 0.04	0.05
S II	-5.66 ± 0.20	-5.05 ± 0.16	-5.62 ± 0.13	-5.13 ± 0.32	-4.83	-4.86 ± 0.05	0.03
Ca II	$-6.02 \pm 0.04^*$	-5.38 ± 0.14	$-5.87 \pm 0.04^*$	$-5.07 \pm 0.03^*$	-5.68	-5.69 ± 0.04	0.01
Sc II	-8.68 ± 0.04	...	-8.94	-8.83 ± 0.10	-0.11
Ti II	-6.52 ± 0.05	-5.87 ± 0.07	-6.58 ± 0.04	-6.55 ± 0.13	-7.05	-7.10 ± 0.06	0.05
Cr I	...	-5.50 ± 0.03	-6.37	-6.36 ± 0.10	-0.01
Cr II	-6.28 ± 0.09	-5.55 ± 0.18	-6.08 ± 0.11	-5.92 ± 0.12	-6.37	-6.36 ± 0.10	-0.01
Mn I	...	-4.44 ± 0.10	-5.07 ± 0.16	-4.38 ± 0.21	-6.65	-6.61 ± 0.03	-0.04
Mn II	-5.81 ± 0.20	-4.51 ± 0.18	-5.08 ± 0.24	-4.36 ± 0.22	-6.65	-6.61 ± 0.03	-0.04
Fe I	-3.98 ± 0.06	-4.91 ± 0.04	-4.60 ± 0.09	-4.33 ± 0.13	-4.37	-4.55 ± 0.05	0.18
Fe II	-3.87 ± 0.14	-4.88 ± 0.12	-4.57 ± 0.09	-4.41 ± 0.17	-4.37	-4.55 ± 0.05	0.18
Fe III	-3.84 ± 0.07	-4.37	-4.55 ± 0.05	0.18
Ni II	...	$-6.46 \pm 0.04^*$	-6.60 ± 0.01	$-6.14 \pm 0.07^*$	-5.79	-5.77 ± 0.04	-0.02
Sr II	$-8.35 \pm 0.03^*$	$-8.61 \pm 0.02^*$	$-9.21 \pm 0.01^*$	$-6.00 \pm 0.04^*$	-9.14	-9.08 ± 0.05	-0.06
Hg I	-6.38 ± 0.28	$-6.13 \pm 0.20^*$	$-6.36 \pm 0.19^*$	$-4.59 \pm 0.35^*$	-10.95	$-10.87 \pm 0.18^{**}$	-0.08
Hg II	-6.53 ± 0.33	$-6.38 \pm 0.20^*$	-6.89 ± 0.19	-5.61 ± 0.13	-10.95	$-10.87 \pm 0.18^{**}$	-0.08

Elements for which abundances are derived from a unique line are marked with an asterisk (*).

[A] and [B] are respectively the chemical solar abundances used in Kurucz (1993) and Grevesse et al. (2007). Hg abundance of [B] marked with double asterisks (**) is obtained from meteorites. The abundance difference between these two sets are listed in column [C].

that by using an atmospheric model calculated with iron abundance [Fe/H] between 1 and 10 times its solar value, the derived abundances for elements can change by up to ± 0.25 dex. Uncertainties in atmospheric parameters (T_{eff} and $\log g$) and in the atomic data can also modify abundances. NLTE effects may also play a role. The errors in the average abundances in Table 3 are obtained by calculating the standard deviation relative to the mean abundance for elements with a large number of lines. The uncertainties in the atmospheric parameters are not included in error calculations for these elements. For those species for which abundances are derived from a unique line, we took the formal error derived from the line profile fit. This error arises from the uncertainties in stellar atmospheric parameters and atomic data. The solar abundances used in this study are those used in Kurucz (1993)(see [A] of Table 3). In the same table, we present the solar abundances determined by Grevesse et al. (2007) ([B]). The differences between these two sets of abundances are summarized in column 8 ([C]) of Table 3 and are within ~ 0.2 dex.

4.1 HD 71066

The elements He, C, O, Mg, Si, P, S, Ca, Ti, Cr, Mn, Fe, Sr and Hg were investigated to determine their abundances in the atmosphere of HD 71066. The abundances are given in col. 2 of Table 3. Comparing these abundances to those of the sun, the elements C, O, Si, Ca, Ti, Cr and Fe are within 0.5 dex of solar values. He, Mg and S are deficient by more than 0.5 dex, while P, Mn, Sr and Hg are overabundant by more than 0.5 dex.

Comparing the Cr abundance derived in this paper to the $\log(N_{Cr}/N_H) = -6.23 \pm 0.10$ obtained by Savanov & Hubrig

(2003), we find a good agreement. The enhanced Fe abundance of 0.11 dex obtained by Hubrig et al. (1999) is consistent with our measurement when taking into account the error bars. Concerning the abundance of Hg, no significant difference is observed between that derived from this study and the value reported by Dolk et al. (2003), namely $\log(N_{Hg}/N_{tot}) = -6.35 \pm 0.26$.

4.2 HD 175640

Chemical abundances of a large number of elements were determined for HD 175640 by Castelli & Hubrig (2004). In this paper, we diagnosed abundances of He, C, O, Mg, Si, P, S, Ca, Ti, Cr, Mn, Fe, Ni, Sr and Hg. The measured abundances are presented in col. 3 of Table 3. The elements C, O, Mg, Si, P, S and Ca show abundances within 0.5 dex of solar values. Helium, iron and nickel are underabundant by more than 0.5 dex, while Ti, Cr, Mn, Sr and Hg are enhanced by more than 0.5 dex.

The abundances obtained in this study are generally in agreement with those derived by Castelli & Hubrig (2004). However, our abundance of Ni is 0.37 dex lower than reported by those authors ($\log(N_{Ni}/N_{tot}) = -6.09 \pm 0.16$). The mercury abundance $\log(N_{Hg}/N_{tot}) = -6.35 \pm 0.15$ derived by Dolk et al. (2003) is close to that reported in this paper. Disagreements are observed between mean abundances derived from the analysis of neutral and singly ionized Hg (0.25 dex) lines. These differences are greater than the error bars associated with these abundances. Potential sources of these differences in the abundances inferred from different ions of an element, which are observed in several of the stars in this study, will be explored in Sect. 6.

Unlike the other stars presented in this paper, the spectrum of

Table 4. The slope a , obtained from a linear regression of abundance vs. optical depth: $\log(N_{ion}/N_{tot}) = a \log \tau_{5000} + b$. The number of lines investigated is represented by n .

Element	HD 71066		HD 175640		HD 178065		HD 221507	
	a	n	a	n	a	n	a	n
S	$+0.043 \pm 0.1761$	15
Ti	$+0.050 \pm 0.061$	28	-0.069 ± 0.025	41	$+0.034 \pm 0.021$	33	$+0.130 \pm 0.143$	14
Cr	$+0.045 \pm 0.065$	19	-0.010 ± 0.046	45	-0.025 ± 0.039	35	$+0.072 \pm 0.079$	12
Mn	$+0.008 \pm 0.038$	62	$+0.289 \pm 0.060$	62	$+0.051 \pm 0.069$	28
Fe	$+0.035 \pm 0.012$	158	$+0.061 \pm 0.018$	57	$+0.052 \pm 0.013$	94	$+0.008 \pm 0.024$	57

HD 175640 does not show any absorption (or emission) line at the location of the Hg II $\lambda 5677$ line.

4.3 HD 178065

Lines of the elements He, C, O, Mg, Si, P, S, Ca, Sc, Ti, Cr, Mn, Fe, Ni, Sr and Hg were analyzed to determine their abundances in the atmosphere of HD 178065. The abundances of the elements C, O, Mg, Si, Ca, Sc, Ti, Cr, Fe and Sr are within 0.5 dex of their corresponding solar values. He, S and Ni are deficient by more than 0.5 dex, while P, Mn and Hg are enhanced by more than 0.5 dex.

The Cr abundance is close to the $\log(N_{Cr}/N_H) = -5.99 \pm 0.10$ obtained by Savanov & Hubrig (2003). A slight difference of 0.14 dex is obtained between the iron abundance derived in this study and the $\log(N_{Fe}/N_{tot}) = -4.43$ obtained by Hubrig & Castelli (2001). The mean abundance of Hg is in good agreement with $\log(N_{Hg}/N_{tot}) = -6.65 \pm 0.12$ derived by Dolk et al. (2003).

As mentioned above, differences of 0.16 dex and 0.53 dex are respectively observed between the abundances of neutral and singly-ionized states of both Mg and Hg.

4.4 HD 221507

For the more rapidly rotating ($v \sin i = 25 \text{ km s}^{-1}$) star HD 221507, we analyzed abundances of He, C, O, Mg, Si, P, S, Ca, Ti, Cr, Mn, Fe, Ni, Sr and Hg. We find that C, O, Mg, Si, S, Ti, Cr, Fe and Ni are within 0.5 dex of the solar abundance. Helium is the only underabundant element, while P, Ca, Mn, Sr and Hg are overabundant by more than 0.5 dex.

As observed in other stars, a difference (of 0.33 dex) is observed between abundances of neutral and singly ionized magnesium. The abundance derived from the Hg I $\lambda 5460.731$ line is enhanced by 1.02 dex with respect to that obtained from Hg II lines.

The Si abundance agrees very well with $\log(N_{Si}/N_{tot}) = -4.5 \pm 0.10$ obtained from UV analysis by Smith (1993). Our result for Mn abundance is consistent with the value ($\log(N_{Mn}/N_H) = -4.5 \pm 0.05$) found by Jomaron et al. (1999) for this star. The iron abundance is in excellent agreement with $\log(N_{Fe}/N_H) = -4.35 \pm 0.10$ obtained by Smith & Dworetzky (1993). Although the Hg II abundance obtained by Dolk et al. (2003) differs by 0.21 ± 0.43 dex compared to our analysis, the values are still within the error bars.

5 STRATIFICATION

For elements exhibiting a sufficiently large number of suitable lines in our spectra, we have examined the dependence of their abundance versus the optical depth of line core formation. To evaluate

vertical stratification, we have calculated the slope a of the abundance versus τ_{5000} by performing a linear fit to the data by the Least Squares Method (LSM): $\log(N_{ion}/N_{tot}) = a \log \tau_{5000} + b$. The slopes a obtained for investigated elements are summarized in Table 4. For the confirmation of vertical stratification, we require that the three following conditions be met:

- (1) More than 10 lines, formed at different optical depths, must be present in the spectra.
- (2) The slope a should be statistically significant in comparison to the uncertainties.
- (3) The chemical abundance should change significantly (by more than ~ 0.5 dex) in the diagnosed range of optical depth.

This last condition is related to the fact that several factors such as errors in atmospheric parameters (T_{eff} and $\log g$), NLTE effects and uncertainties in the model atmosphere can cause errors in abundance determination. For example, as discussed by Takada-Hidai (1991), an error of ± 1000 K in T_{eff} causes errors in abundances derived from resonance lines by ± 0.08 dex and $[-0.19, +0.25]$ dex for lines with high excitation energy. Furthermore, an error of ± 0.3 dex in $\log g$, introduces uncertainties in abundance calculations of ± 0.1 dex. The uncertainty in the metallicity can account for an error of ~ 0.25 dex for abundance calculations (Khan & Shulyak 2007). Requiring a significant change in abundance helps ensure that any abundance gradient is real, and not generated by poorly-quantified uncertainties.

5.1 HD 71066

In the spectrum of HD 71066, lines of Ti, Cr and Fe were studied for vertical stratification. We found that titanium lines are formed over a small range of optical depth, between $\log \tau_{5000} \approx -5.9$ and -5.3 (see Fig. 4a). The slope a is relatively small compared to the formal uncertainty (see Table 4). We conclude that the titanium abundance does not show a significant dependence on optical depth for HD 71066.

As reported in Table 4, the linear fit of chromium abundance versus optical depth reveals a slope smaller than the error. No significant variation of Cr abundance in the optical depth range from $\log \tau_{5000} \approx -5.9$ to -4.8 is detected (see Fig. 4b).

From $\log \tau_{5000} \approx -5.5$ to -1 , the iron abundance (derived from 22 Fe I, 134 Fe II and 2 Fe III lines) does not show a clear dependence on depth (see Fig. 4c). The LSM gives a slope which is marginally significant compared to the error ($a \approx 3\sigma_a$). However, the variation of the abundance versus the optical depth is too weak to confidently conclude that Fe is stratified in the atmosphere of HD 71066.

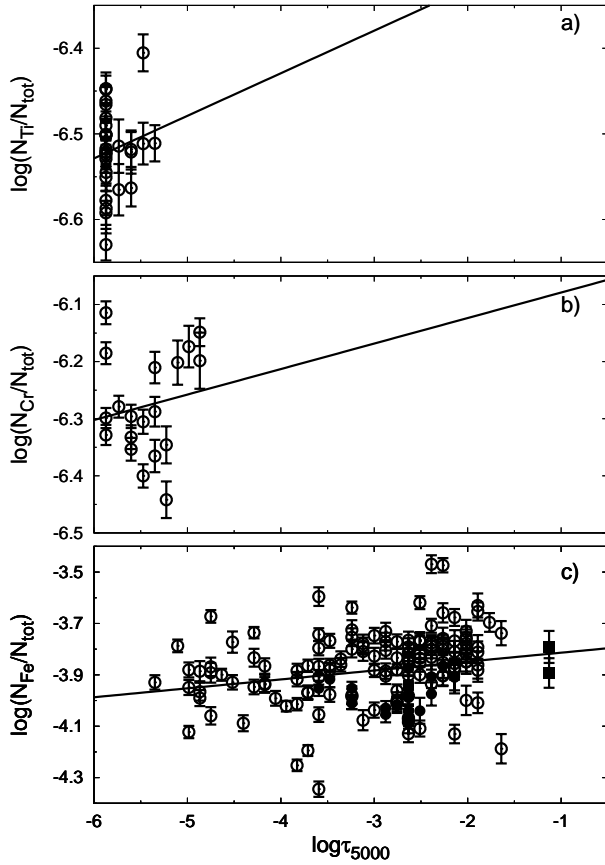


Figure 4. Dependence of a) Ti, b) Cr and c) Fe abundance in the atmosphere of HD 71066 against the line (core) formation optical depth calculated at $\lambda = 5000 \text{ \AA}$. The optical depth range between -6 and -0.5 is approximately associated to the physical depth from ~ 0 to $9.58 \times 10^3 \text{ km}$. The filled circles, open circles and filled squares correspond respectively to abundances derived from the neutral, singly and doubly ionized ions. The error bars correspond to formal uncertainties derived from the fits of line profiles. The linear fit of the data using the least squares method $\log(N_{ion}/N_{tot}) = a \log \tau_{5000} + b$ is represented by the solid line.

5.2 HD 175640

In the spectrum of HD 175640, lines of S, Ti, Cr, Mn and Fe were studied for vertical stratification. With 15 S II lines, we were able to evaluate the possibility of stratification of this element in the atmosphere of HD 175640. As the slope a is lower than the corresponding error, sulfur shows no sign of stratification between $\log \tau_{5000} \approx -2.4$ and -1.2 (see Fig. 5a).

The linear fit of Ti abundance versus the optical depth of HD 175640 reveals a weak (negative) slope. No significant variation of Ti abundance is observed in the optical depth range from $\log \tau_{5000} \approx -5.9$ to -4.6 of HD 175640 in Fig. 5b.

Forty-five Cr lines were studied in the spectrum of HD 175640, of which 2 are from the neutral ion. The chromium abundance presented in Fig. 5c does not show any variation with optical depth ranging between $\log \tau_{5000} \approx -5.9$ and -3.6 . The slope $a \approx 0.2\sigma_a$ is not statistically significant and is very weak. No stratification is thus observed.

Fig. 5d shows the variation of Mn abundance with optical depth between $\log \tau_{5000} \approx -4.1$ and -1 . The slope obtained from the linear fit of Mn abundance in the atmosphere of HD 175640

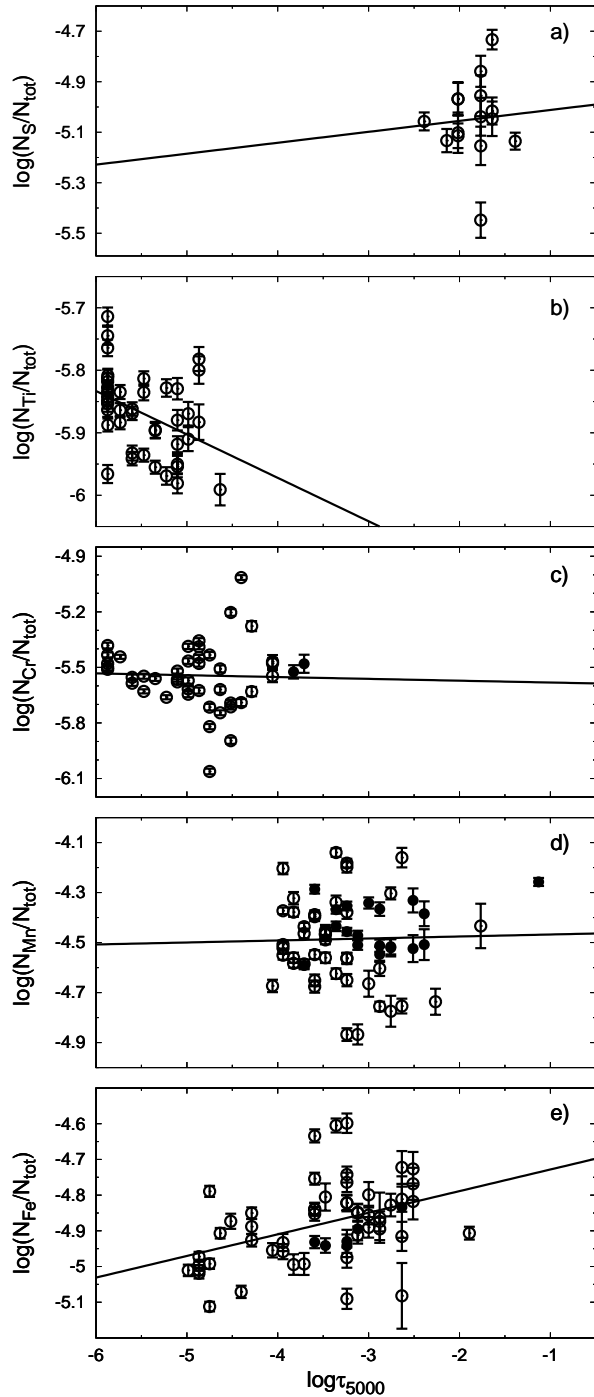


Figure 5. Same description as in Fig. 4 but for a) S, b) Ti, c) Cr, d) Mn and e) Fe for HD 175640.

is relatively weak and is statistically not significant ($a \approx 0.2\sigma_a$). Manganese is not stratified in the atmosphere of HD 175640.

The investigation of 6 Fe I and 51 Fe II lines yields a weak slope (see Table 4) between $\log \tau_{5000} \approx -5$ and -1.8 . We conclude that iron is not detectably stratified in the diagnosed optical depths of the atmosphere of HD 175640 (see Fig. 5e).

5.3 HD 178065

In the spectrum of HD 178065, lines of Ti, Cr, Mn and Fe were studied for vertical stratification. Fig. 6a shows that the titanium lines observed are formed in a small range of optical depth (between $\log \tau_{5000} \approx -5.9$ and -4.8). The slight slope (see Table 4) leads us to conclude that Ti is not significantly stratified in the diagnosed optical depths of HD 178065.

As presented in Table 4, the linear fit of Cr abundance in the investigated optical depth of HD 178065 reveals a negative slope. However, this slope is weaker than the associated error ($a \approx 0.6\sigma_a$). The chromium abundance does not show a systematic dependence on optical depth from $\log \tau_{5000} \approx -5.9$ to -4.2 (see Fig. 6b).

The abundance obtained from 5 Fe I and 89 Fe II lines also does not reveal a significant variation at optical depths between $\log \tau_{5000} \approx -5$ and -2 (see Fig. 6d). The slope a is relatively small (see Table 4), and we conclude that iron is not detectably stratified in the atmosphere of HD 178065 in the diagnosed optical depths.

In contrast to the behaviour observed for Ti, Cr and Fe, Fig. 6c shows a strong increase of the Mn abundance with optical depth. The slope $a \approx 5\sigma_a$ is statistically significant, and the inferred Mn abundance increases by ~ 0.7 dex in the diagnosed range of optical depth between $\log \tau_{5000} \approx -4.5$ and -2.5 . Therefore Mn satisfies all 3 of our criteria required for the detection of stratification.

To confirm the presence of Mn stratification, several tests have been undertaken. We began by verifying the effect on the derived stratification of modifying T_{eff} and the metallicity.

First, we determined the abundance and stratification of Mn using ATLAS9 model atmospheres with different effective temperatures centered on the adopted effective temperature of HD 178065 (11 000 K, 11 500 K, 12 500 K and 13 000 K). Neutral Mn lines are sensitive to the change of T_{eff} . A difference of ± 1000 K (3-4 times larger than our estimate of the uncertainty associated with T_{eff}) changes the abundance by approximately ± 0.6 dex. In contrast, the difference is less than ~ 0.2 dex for Mn II lines. At each adopted effective temperature, the slopes remain statistically significant for Mn I (larger than $3\sigma_a$) and Mn II (larger than $4\sigma_a$), as well as for all Mn lines (at least $4\sigma_a$). The increase of the Mn abundance is also large enough (more than 0.5 dex) to be considered numerically significant.

Secondly, we analyzed Mn lines using ATLAS9 atmosphere models with $T_{\text{eff}} = 12\,000$ K, calculated with different metallicities from ± 0.1 to ± 1 dex. These metallicities correspond to both deficiencies (negative) and enrichments (positive) of metals relative to the sun denoted by $[+0.0]$. The Mn abundances determined with different metallicities are not very different in comparison to those obtained with the solar metallicity model. The slopes of the regression of Mn abundance versus optical depth increase when metallicity increases. As an example, for $[-1.0]$, the slope obtained is $+0.240 \pm 0.066$, $+0.289 \pm 0.060$ for $[+0.0]$, and $+0.326 \pm 0.058$ for $[+1.0]$. These remain both statistically and quantitatively significant for all investigated metallicities.

Thirdly, we have analyzed the Mn lines using a model atmosphere computed with a different code: an LTE model obtained with the Phoenix code (Hauschildt et al. 1997). This model is calculated by assuming $T_{\text{eff}} = 12\,193$ K, $\log g = 3.54$ while using the abundances given in Table 3. Mean abundances derived from Mn I and Mn II lines are respectively -5.17 ± 0.18 and -5.08 ± 0.23 . No disagreement is observed between abundances derived from Mn II lines using the two different atmosphere models, while for Mn I, the difference is within the error bars. The slope $a = +0.296 \pm 0.061$ obtained from the regression of Mn versus the optical depth using

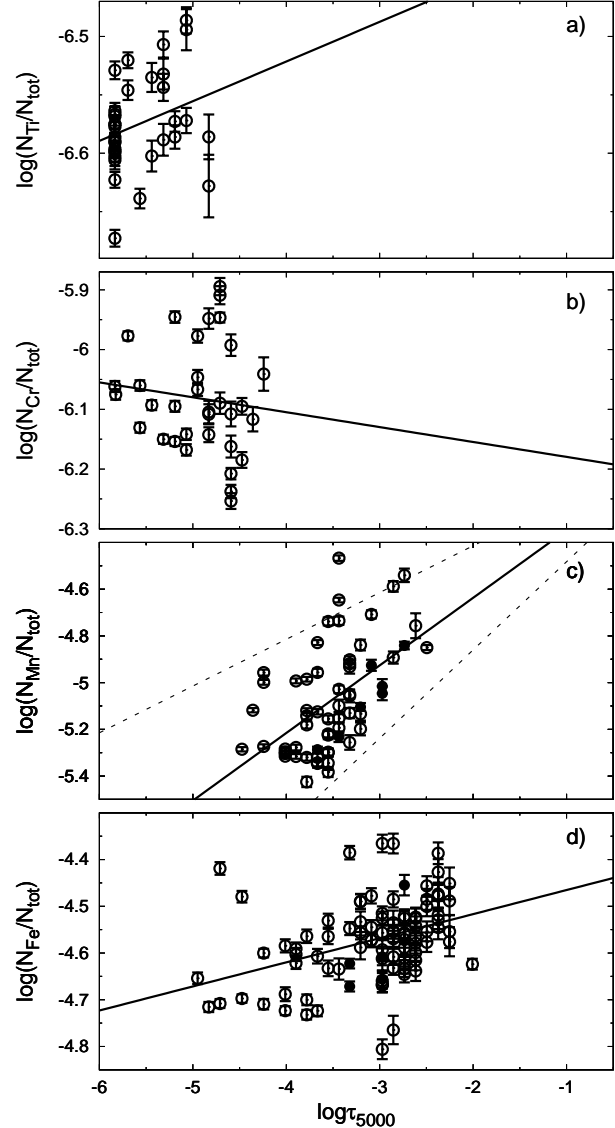


Figure 6. Same description as in Fig. 4 but for a) Ti, b) Cr, c) Mn and d) Fe for HD 178065, but where we have added 3σ regression curves (dash) for Mn.

the Phoenix atmosphere model is close to those obtained with ATLAS9.

We therefore conclude that the Mn stratification remains statistically significant for both ATLAS9 and Phoenix model atmospheres, at all investigated effective temperatures and metallicities. As the variation of Mn abundance is substantial, we can confidently claim that Mn is stratified in the atmospheric layers of HD 178065.

Following the detection and modeling of stratification in magnetic Ap stars by Babel (1994), vertical abundance profiles were subsequently parametrized assuming a simple two-step (or two-zone) model (Wade et al. 2001b; Ryabchikova et al. 2003). In an attempt to characterize the vertical distribution of Mn in the atmosphere of HD 178065, we have selected the best line profiles candidates to fit simultaneously using synthetic profiles computed assuming the two-step model. We assume an abundance $\log(N_{\text{ion}}/N_{\text{tot}})_1$ deep in the atmosphere, below optical depth τ_1 . The abundance in the upper atmospheric layers (above optical depth τ_2) is given by $\log(N_{\text{ion}}/N_{\text{tot}})_1 + \Delta\epsilon$, where $\Delta\epsilon$ is the dif-

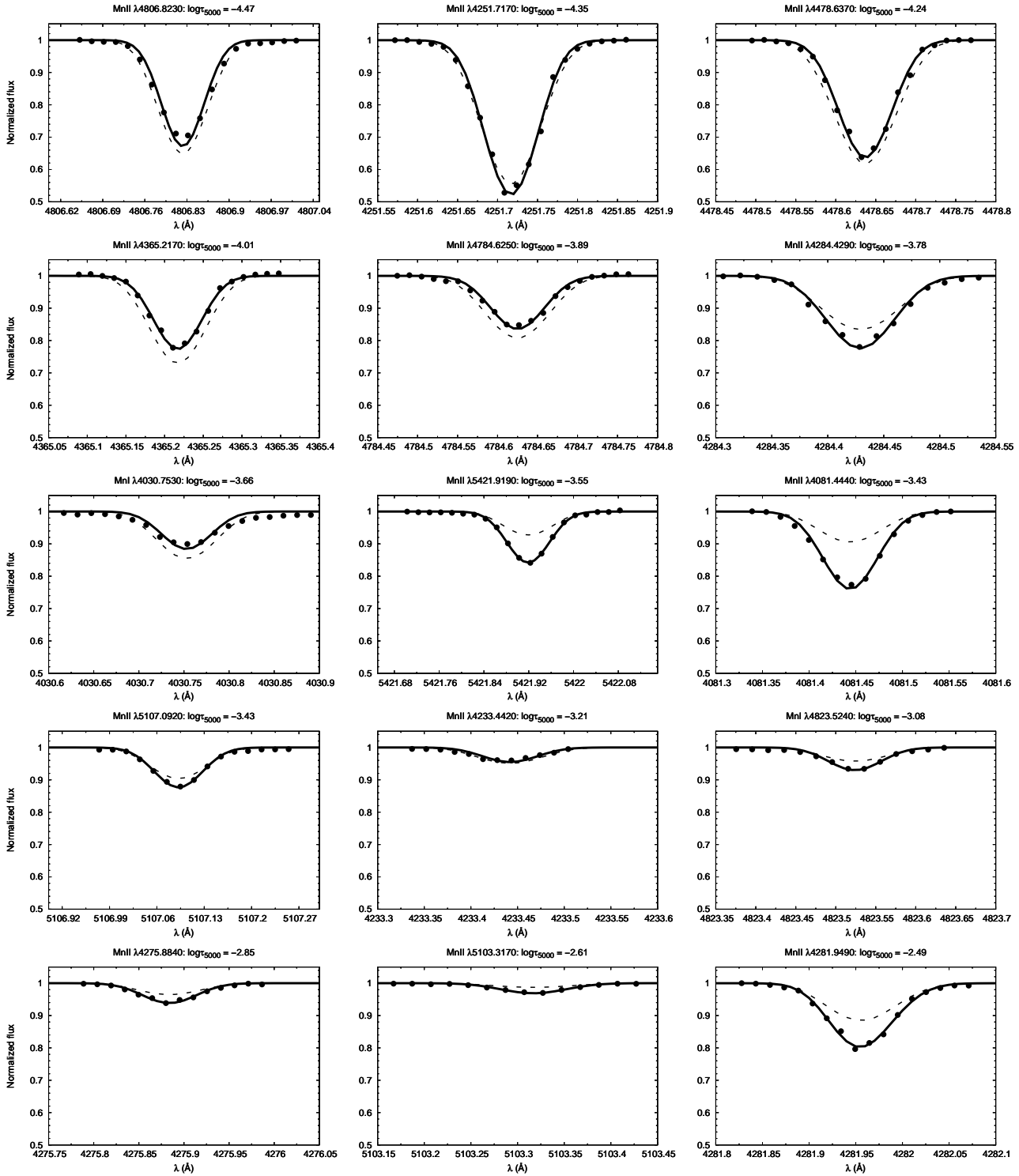


Figure 7. A sample of manganese lines observed (dots) for HD 178065. These lines are fitted by assuming an uniform abundance (dashed curve) and a stratified one (solid curve). The optical depth of line core formation is also given for each line.

ference in abundance between the deeper and upper zones. The atmospheric layers between τ_1 and τ_2 (the “transition zone”) are assumed to have abundances given by a linear interpolation between that of the deep layers and of the upper layers. In our fitting of the line profiles, this method operates with six free parameters ($\log(N_{ion}/N_{tot})_1$, $\Delta\epsilon$, τ_1 , τ_2 , V_r and $\nu \sin i$) which are simul-

taneously fitted to all selected lines. More details concerning this method are provided by Khalack et al. (2007).

We simultaneously analyzed the selected Mn line profiles, and the results of the line synthesis are presented in Table 5 and the derived stratification profile is represented in Fig. 8. Fig. 7 shows some Mn II lines formed at different optical depths. These line profiles are fitted by assuming an uniform abundance (dashed curve)

Table 5. Results obtained from the simultaneous analysis of manganese lines of HD 178065 by assuming a two-step model. The variables τ_1 and τ_2 are the optical depths where the abundance of Mn decreases linearly by $\Delta\epsilon$. The quality of the fit for the uniform and stratified models are respectively represented by χ_{UM}^2 and χ_{SM}^2 .

$\log(N_{\text{Mn}}/N_{\text{tot}})_1$	$\Delta\epsilon$	$\log \tau_1$	$\log \tau_2$	V_r (km s ⁻¹)	$v \sin i$ (km s ⁻¹)	χ_{UM}^2	χ_{SM}^2
-4.47 ± 0.10	-0.74 ± 0.21	-2.92 ± 0.10	-3.79 ± 0.20	34.70 ± 0.10	1.52 ± 0.03	13.53	4.82

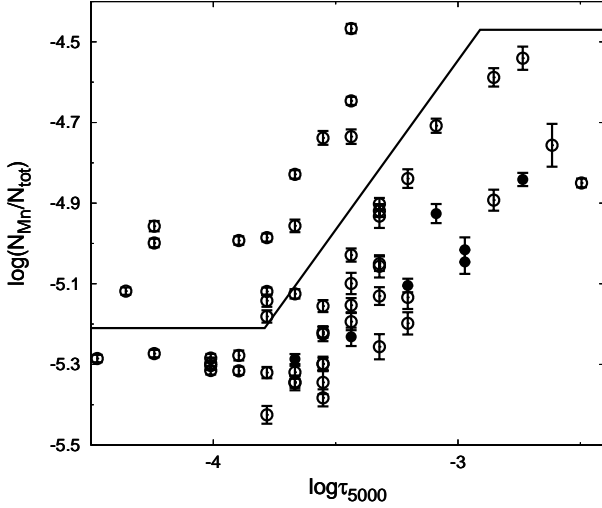


Figure 8. The manganese stratification profile in the atmosphere of HD 178065.

and a stratified abundance (solid curve). The reduced χ^2 for the uniform and stratified models are summarized respectively in columns 7 and 8 of Table 5. As represented in Fig. 8, the abundance of Mn increases deep in the atmosphere of HD 178065 by 0.74 ± 0.21 dex in the optical depth range between -3.79 ± 0.20 and -2.92 ± 0.10 . The abundance of Mn is larger in the lower atmosphere as compared to the shallower atmosphere. The Mn transition zone observed in HD 178065 dominates the stratified profile. This profile differs strongly from those of Ap stars where the transition zone has a very small extent (Ryabchikova et al. 2005). The radial V_r and rotational $v \sin i$ velocities are similar to those adopted from the individual line analysis discussed in Sect. 3.

5.4 HD 221507

In the spectrum of HD 221507, lines of Ti, Cr, Mn and Fe were studied for vertical stratification. The linear fit of the abundance derived from 14 Ti lines reveals a large slope. However, this slope is heavily weighted by a few lines which are concentrated close to the $\log \tau_{5000} \approx -5.9$. Also, the lines studied here are formed in a small range of optical depth from $\log \tau_{5000} \approx -5.9$ to -5 (see Fig. 9a). Therefore, it is not possible to conclude from these results that Ti is stratified.

From $\log \tau_{5000} \approx -5.9$ to -4.5 , the Cr abundance does not show dependence on depth (see Fig. 9b). The slope obtained ($a \approx 0.9 \sigma_a$) is not statistically significant. Chromium does not show any stratification in the studied optical depth range.

From Mn I and Mn II lines, we obtain no significant slope from the regression. Manganese does not appear to be stratified in the optical depths between $\log \tau_{5000} \approx -4.4$ and -2.2 in HD 221507 (see Fig. 9c).

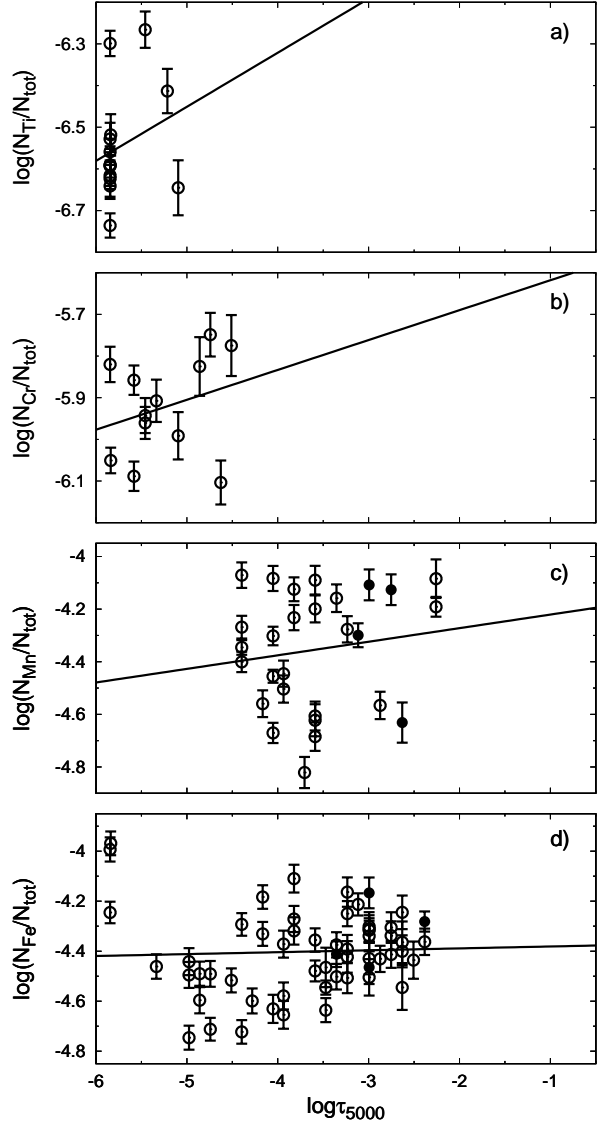


Figure 9. Same description as in Fig. 4 but for a) Ti, b) Cr, c) Mn and d) Fe for HD 221507.

The investigated Fe lines are formed between $\log \tau_{5000} \approx -5.9$ and -2.3 (see Fig. 9d). The linear fit of iron abundance reveals a weak slope (see Table 4) that is not statistically significant.

6 DISCUSSION AND CONCLUSION

In this paper, we determined the abundances of 16 elements in the atmospheres of the HgMn stars HD 71066, HD 175640, HD 178065 and HD 221507. Mean abundances of elements, rel-

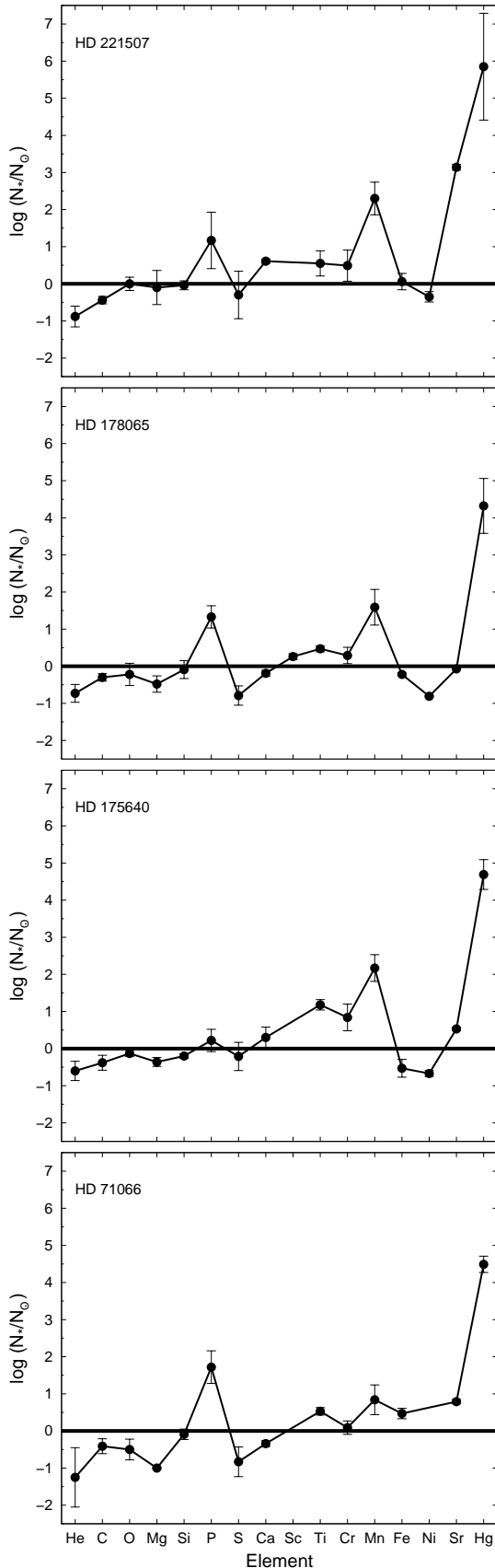


Figure 10. Catalogue of the abundances measured in the atmospheres of HD 71066, HD 175640, HD 178065 and HD 221507. These abundances are relative to the sun, which is represented by the horizontal line.

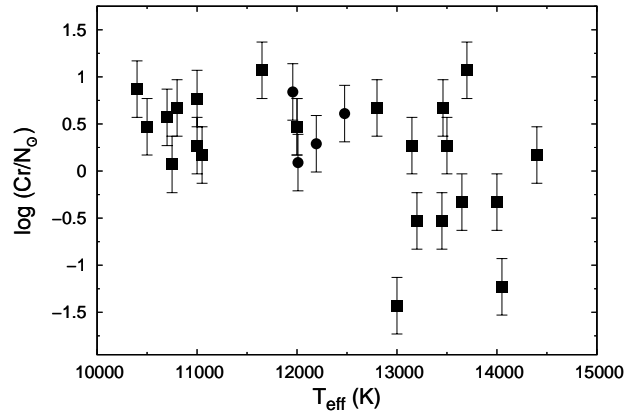


Figure 11. The abundance of Cr against the effective temperature of several HgMn stars. The filled circles and the filled squares correspond respectively to the abundances derived in our study and those of Smith & Dworetsky (1993).

ative to the sun, are presented for each star in Fig. 10. The abundances of most of these elements had never been determined in the past for these stars. However, for the elements previously investigated and discussed in Sec. 4, the mean abundances obtained are generally in good agreement with past studies.

As expected (see Fig. 10), He is underabundant while Mn and Hg are overabundant in all the investigated stars. Phosphorus, which is generally overabundant in HgMn stars, is solar in HD 175640. Titanium and chromium, which are typically present in their solar abundances in HgMn stars, are strongly enhanced in the atmosphere of HD 175640. We also notice that the more rapidly rotating star HD 221507 presents the highest abundances of Sr and Hg of our sample.

We have examined the dependence of the mean abundances of each element as a function of the physical parameters T_{eff} and $v \sin i$. As the results we obtained are derived from only four data points with highly clustered T_{eff} and $v \sin i$, we decided to use data from published papers. We used Ryabchikova (1998) for P and Sr, Smith & Dworetsky (1993) for Cr, and Smith (1997) for Hg. We can definitely confirm the correlation of the abundance of Cr versus T_{eff} (see Fig. 11), with a large dispersion of abundances for $T_{\text{eff}} \geq 13\,000$ K (Smith & Dworetsky, 1993). However, we can not confidently affirm any trends of the abundance of P with respect to T_{eff} , and Sr and Hg with respect to $v \sin i$.

The synthesis of elements represented by a large number of lines in our spectra allowed us to track vertical stratification of elements in the atmospheres of these stars. As shown in Sec. 5, an attempt to detect stratification for Ti, Cr and Fe in HD 71066, S, Ti, Cr, Mn and Fe in HD 175640, Ti, Cr, Mn and Fe in HD 178065 and Ti, Cr, Mn and Fe in HD 221507 was undertaken. Most of these elements' abundances do not show any significant tendencies in the diagnosed optical depths.

The study of Savanov & Hubrig (2003) that reports the vertical stratification of Cr in 10 HgMn stars, is performed in the spectral region $4812.34 - 4864.33$ Å. They did not evaluate the depth of line formation. The spectra used in our study do not appear to be of sufficient quality to confidently detect the chromium abundance variation claimed by those authors. Therefore, it is difficult to compare their data with the results presented here.

An interesting finding is that Fe increases slightly (~ 0.25 dex) with optical depth for the four stars (HD 71066,

HD 175640, HD 178065 and HD 221507). This systematic trend for Fe might suggest stratification. However the increase in abundance is too small to confidently conclude to the detection of stratification.

Strong evidence of Mn stratification in the atmosphere of HD 178065 is observed. The abundance of Mn increases by ~ 0.7 dex in diagnosed optical depth range. The simultaneous fit of lines assuming a two-step model also shows that Mn increases towards the deep atmosphere. If such stratification can be confirmed (for Mn or for other elements), this would provide important new quantitative constraints on diffusion in the atmosphere of HgMn stars. Such observed vertical stratification profiles could then be compared to theoretical model atmospheres which include elemental stratification such as those of Hui-Bon-Hoa et al. (2000).

Differences observed between the abundance of neutral and ionized Mg ions are greater than 0.1 dex in HD 178065 and HD 221507. The largest disagreements are observed between Hg I and Hg II in HD 175640, HD 178065 and HD 221507, where they are greater than 0.25 dex. This result remains the same even when not using the isotopic data for the Hg II λ 3984 line shown in Fig. 2. The fact that differences are observed for some stars and not for others lets us to conclude that they may not be only attributed to uncertainties surrounding atomic data and/or small number of lines observed. The sources of these differences might be attributed to NLTE effects. Takada-Hidai (1991) showed that neutral ions are more affected by NLTE corrections than ionized ones in HgMn stars. However, NLTE corrections are smaller for the heavier ions (Takada-Hidai 1991). Basing on the aforementioned paper, the magnitudes of NLTE corrections for some elements are -0.4 dex for Be II, from -2.00 dex to 0.00 dex for O I, -0.02 dex for Mg I, -0.04 dex for Mg II, from -0.45 dex to $+0.70$ dex for Ca II, $+0.20$ dex for Sr II and from -0.3 dex to $+0.3$ dex for Ba II. The corrections are given to indicate possible uncertainties in our results. After the discovery of Ga ionization anomalies in HgMn stars by Smith (1995), this author suggested stratification as the possible cause of these anomalies.

In this paper, we reported for the first time the detection of Mn stratification in a HgMn type star. However, the attempt to detect element stratification failed for most of the investigated elements. The investigation of HgMn stars could be complicated by several physical process, which should be taken into account. Sigut (2001) suggested that the emission lines present in spectra of some HgMn stars are photospheric in nature. After the first discovery of Mn II emission lines in the spectra of the HgMn star HD 186122 (46 Aql) by Sigut et al. (2000), emission lines of several elements were also discovered (Wahlgren & Hubrig 2000). These authors observed titanium and chromium emission lines in the spectra of HD 71066, HD 175640 and HD 178065. As interpreted by Sigut (2001), the presence of emission lines is caused by interlocked NLTE effects in the region where the element is stratified. When doing LTE analysis such as done in this paper, the presence of such emission lines increases the uncertainty of their results.

Possible presence of spots and weather in the atmosphere of HgMn stars also add complications to the investigation of these stars. The variability of Hg II λ 3984 in the spectra HgMn stars is interpreted as inhomogeneous distribution of this element on the stellar surface (Adelman et al. 2002; Kochukhov et al. 2005). To properly study this line, isotopic consideration is critical. Several line profile variations are found in other HgMn stars, such as the strong line variations of Pt, Hg, Sr, Y, Zr, He and Nd in the eclipsing binary AR Aur by Hubrig et al. (2006).

We notice here the absence of the mercury line (Hg II λ 5677)

in the spectrum of HD 175640. This means that the conditions required for the formation of the absorption or the emission Hg II λ 5677 line are not met in the specific layers. On the other hand, it could also mean that the absorption line is formed in deeper layers, but the emission line forms in upper layers and fills in the line. This adds a constraint to the hypothesis that NLTE effects probably act in the atmosphere of HD 175640. In future studies, improvements must be brought to the characterization of the optical depth of line formation and inclusion of NLTE effects. The study of spectral regions covering the UV and IR may allow to diagnose deeper and shallower regions of the atmospheres. Also, spectra with a high S/N and accurate atomic data might permit us to detect weaker stratification.

ACKNOWLEDGMENTS

We thank ESO for the availability of the spectra used in this work. We would like to thank J.D. Landstreet and V. Tsybal for useful discussions, as well as spectra and codes they have made available to us. Thanks to Réseau Québécois de Calcul de Haute Performance (RQCHP) for computationnal resources. This research was partially supported by NSERC. GAW is supported by the Academic Research Programme of the Canadian Department of National Defence. FL thanks the Faculté des Études Supérieures et de la Recherche de l'Université de Moncton for financial support. We thank the referee for the helpful comments.

REFERENCES

- Abt H.A., Chaffee F.H., Suffolk G., 1972, *ApJ*, 175, 779
- Adelman S.J., Gulliver A.F., Kochukhov O.P., Ryabchikova T.A., 2002, *ApJ*, 575, 449
- Adelman S.J., 1994, *MNRAS*, 266, 97
- Alecian G., 1982, *A&A*, 107, 61
- Aller M.F., 1970, *A&A*, 6, 67
- Babel J., 1994, *A&A*, 283, 189
- Balona L.A., 1994, *MNRAS*, 268, 119
- Castelli F., Hubrig S., 2004, *A&A*, 425, 263
- Cowley C.R., Hubrig S., González G.F., Nuñez N., 2006, *A&A*, 455, L21
- Dolk L., Wahlgren G.M., Hubrig S., 2003, *A&A*, 402, 299
- Dubaj D., Monier R., Alecian G., LeBlanc F., 2004, *Semaine de l'Astrophysique Française*, meeting held in Paris, France, June 14-18, 2004. Edited by F. Combes, D. Barret, T. Contini, F. Meynadier and L. Pagani. Published by EdP-Sciences, Conference Series, 287
- Gerbaldi M., Floquet M., Hauck M., 1985, *A&A*, 146, 341
- Grevesse N., Asplund M., Sauval A.J., 2007, *SSR*, 130, 105
- Hauschildt P.H., Baron E., Allard F., 1997, *ApJ*, 483, 390
- Heacox W.D., 1979, *AJSS*, 41, 675
- Holt R.A., Scholl T.J., Rosner S.D., 1999, *MNRAS*, 306, 107
- Hubrig S., González, J.F., Savanov, I., et al., 2006, *MNRAS*, 371, 1953
- Hubrig S., Castelli F., 2001, *A&A*, 375, 963
- Hubrig S., Castelli F., Wahlgren G.M., 1999, *A&A*, 346, 139
- Hui-Bon-Hoa A., LeBlanc F., Hauschildt P.H., 2000, *ApJ*, 535, L43
- Jomaron C.M., Dworetzky M.M., Allen C.S., 1999, *MNRAS*, 303, 555

- Khalack V.R., LeBlanc F., Behr B.B., Wade G.A., Bohlender D., 2008, *A&A*, 477, 641
- Khalack V.R., LeBlanc F., Bohlender D., Wade G.A., Behr B.B., 2007, *A&A*, 466, 667
- Khan S.A., Shulyak D.V., 2007, *A&A*, 469, 1083
- Kochukhov O., Piskunov N., Sachkov M., Kudryavtsev D., 2005, *A&A*, 439, 1093
- Kupka F., Piskunov N., Ryabchikova T.A., Stempels H.C., Weiss W.W., 1999, *A&A*, 138, 119
- Kurucz R., 1994, CDROM Model Distribution, SAO
- Kurucz R., 1993, CDROM Model Distribution, SAO
- Landstreet J.D., 1998, *A&A*, 338, 1041
- Landstreet J.D., 1988, *ApJ*, 326, 967
- Landstreet J.D., 1982, *ApJ*, 258, 639
- Lanz T., Artru M.-C., Didelon P., Mathys G., 1993, *A&A*, 272, 465
- Martin G.A., Fuhr J.R., Weise W.L., 1988, *J. Phys. Chem. Ref. Data*, 17, Suppl. 3
- Martin W.C., Zalubas R., Musgrove A., 1985, *J. Phys. Chem. Ref. Data*, 14, 751
- Mathys G., Hubrig S., 1995, *A&A*, 293, 810
- Michaud G., 1970, *ApJ*, 160, 641
- Pickering J.C., Thorne A.P., Perez R., 2001, *ApJS*, 132, 403
- Preston G.W., 1974, *ARA&A*, 12, 257
- Ralchenko Yu., Jou F.-C., Kelleher D.E., et al., 2007, NIST Atomic Spectra Database (version 3.1.3)
- Ryabchikova T.A., Leone F., Kochukhov O., 2005, *A&A*, 438, 973
- Ryabchikova T.A., Wade G.A., LeBlanc F., 2003, *Proc. of 210th IAU Symp. on Modelling of Stellar Atmospheres*, ed. N. Piskunov, W.W. Weiss, & D.F. Gray. Published on behalf of the IAU by the Astronomical Society of the Pacific, p.301
- Ryabchikova T.A., Piskunov N.E., Stempels H.C., Kupka F., Weiss W.W., 1999, *Proc. of the 6th International Colloquium on Atomic Spectra and Oscillator Strengths*, Victoria BC, *Physica Spectra T83*, 162
- Ryabchikova T.A., 1998, *Contributions of the Astronomical Observatory Skalnaté Pleso*, vol. 27, no. 3, 319
- Savanov I., Hubrig S., 2003, *A&A*, 410, 299
- Schaller G., Schaerer D., Meynet G., Maeder A., 1992, *A&A*, 96, 269
- Shorlin S.L.S., Wade G.A., Donati J.-F., et al., 2002, *A&A*, 392, 637
- Sigut T.A.A., 2001, *A&A*, 377, L27
- Sigut T.A.A., Landstreet J.D., Shorlin S.L.S., 2000, *ApJ*, 530, 89
- Smith K.C., 1997, *A&A*, 319, 928
- Smith K.C., 1995, *A&A*, 297, 237
- Smith K.C., Dworetsky M.M., 1993, *A&A*, 274, 335
- Smith K.C., 1993, *A&A*, 276, 393
- Takada-Hidai M., 1991, *Evolution of Stars: The Photospheric Abundance Connection IAUS 145*, eds. Michaud G., & Tutukov A., 137
- Wade G.A., Aurière M., Bagnulo S., Donati J.-F., et al., 2006, *A&A*, 451, 293
- Wade G.A., Bagnulo S., Kochukhov O., et al., 2001a, *A&A*, 374, 265
- Wade G.A., Ryabchikova T.A., Bagnulo S., Piskunov N., 2001b, *Magnetic Fields Across the Hertzsprung-Russell Diagram*, ed. G. Mathys, S.K. Solanki, & D.T. Wickramasinghe, *ASP Conf. Ser.*, 248, 341
- Wahlgren G.M., Hubrig S., 2000, *A&A*, 362, L13
- White R.E., Vaughan A.H., Preston G.W., Swings J.P., 1976, *ApJ*

204, 131

This paper has been typeset from a $\text{\TeX}/\text{\LaTeX}$ file prepared by the author.

Table 6. The hyperfine structure of the Mn II λ 4206 line taken from Holt et al. (1999).

λ (Å)	$\log gf$
4206.2960	-4.5828
4206.2980	-3.3653
4206.2994	-2.6963
4206.3111	-4.4367
4206.3136	-3.1746
4206.3156	-2.5872
4206.3306	-4.5238
4206.3337	-3.1211
4206.3362	-2.4777
4206.3545	-4.8517
4206.3582	-3.1626
4206.3613	-2.3729
4206.3872	-3.3534
4206.3909	-2.2742
4206.4249	-2.1814

Table 7. The isotopic composition of the Hg II λ 3984 line taken from Dolk et al. (2003).

Isotope	λ (Å)	$\log gf$
¹⁹⁶ Hg	3983.7710	-4.550
¹⁹⁸ Hg	3983.8386	-2.730
^{199a} Hg	3983.8437	-2.880
^{199b} Hg	3983.8527	-2.740
²⁰⁰ Hg	3983.9124	-2.370
^{201a} Hg	3983.9316	-3.050
^{201b} Hg	3983.9414	-2.810
²⁰² Hg	3983.9932	-2.250
²⁰⁴ Hg	3984.0724	-2.880

Table 8. Isotopic mixture of the Hg II λ 3984 line for the studied stars.

HD	Isotopic mixture						
	196	198	199	200	201	202	204
71066	1.1	4.0	3.4	15.2	66.9	8.1	1.3
175640	0.0	9.6	8.4	29.2	6.2	43.3	3.3
178065	0.0	5.7	15.2	29.9	2.0	24.0	23.2
221507	0.0	10.0	8.5	10.0	6.6	30.2	34.7

Table 9. Atomic data used for the spectral synthesis. The columns denoted by 1, 2, 3 and 4 are respectively the abundances measured in the atmospheres of HD 71066, HD 175640, HD 178065 and HD 221507. The source of the atomic data is mostly VALD, unless some other sources are specified in column 10. The damping parameters $\log \gamma_{\text{rad}}$ and $\log \gamma_{\text{St}}$ which are not available are represented by a horizontal line.

λ (Å)	E_i (eV)	$\log gf$	$\log \gamma_{\text{rad}}$	$\log \gamma_{\text{St}}$	1	2	3	4	Sources
C II									
3918.9702	16.3320	-0.533	8.980	-4.930	-3.96	-3.86	-3.78		
4267.2590	18.0460	0.717	9.390	-4.760	-3.82			-3.92	
O I									
3947.2928	9.1460	-2.096	6.660	-4.700	-3.74		-3.54		
3947.4827	9.1460	-2.244	6.660	-4.700		
3947.5827	9.1460	-2.467	6.660	-4.700		
5436.8588	10.7410	-1.398	7.600	-3.820		-3.30			
6155.9664	10.7400	-1.363	7.600	-3.960	-3.66	-3.25			
6155.9664	10.7400	-1.011	7.610	-3.960	-3.22		
6155.9864	10.7400	-1.120	7.610	-3.960		
6156.7362	10.7410	-1.488	7.610	-3.960	-3.69				
6156.7562	10.7410	-0.899	7.610	-3.960	...	-3.20	-3.26		
6156.7761	10.7410	-0.694	7.620	-3.960		
6158.1758	10.7410	-0.996	7.620	-3.960	-3.56	-3.22	-3.30	-3.11	
6158.1858	10.7410	-0.409	7.610	-3.960	
6454.4462	10.7410	-1.066	7.660	-4.280	-3.39				
Mg I									
5172.6840	2.7120	-0.402	7.990	—		-4.78	-4.86		
5183.6040	2.7170	-0.180	7.990	—				-4.40	
Mg II									
3848.2110	8.8640	-1.590	—	—			-5.04		
3848.3410	8.8640	-2.540	—	—			...		
4384.6370	9.9960	-0.790	—	-4.070	-5.47	-4.85	-4.99	-4.57	
4390.5140	9.9990	-1.490	—	-4.070	-5.45	-4.85	-5.04	-4.92	
4390.5720	9.9990	-0.530	—	-4.070	
4427.9940	9.9960	-1.210	—	-4.400			-4.99		
4481.1260	8.8640	0.740	—	—	-5.45	-4.86		-4.67	
4481.1500	8.8640	-0.560	—	—	
4481.3250	8.8640	0.590	—	—	
Si II									
3853.6650	6.8580	-1.517	8.080	-5.150	-4.65	-4.68	-4.59	-4.45	
3856.0180	6.8590	-0.557	8.080	-5.150	-4.58	-4.66	-4.46	-4.48	
3862.5950	6.8580	-0.800	8.080	-5.150	-4.58	-4.69	-4.43	-4.59	
3954.3000	12.5250	-1.040	—	—			-4.83		
3954.5040	12.5250	-0.880	—	—			...		
4075.4520	9.8390	-1.403	—	—		-4.72	-4.67		
4130.8720	9.8390	-0.824	9.440	-4.870	-4.62		-4.57	-4.53	
4130.8940	9.8390	0.476	9.440	-4.870	
5041.0240	10.0670	0.291	9.030	-4.780	-4.55				
5055.9840	10.0740	0.593	9.040	-4.780	-4.64	-4.70			
5056.3170	10.0740	-0.359	9.040	-4.780	-4.64	-4.73			
5466.4610	12.5250	-0.200	9.020	-3.850			-4.62		
5957.5590	10.0670	-0.301	8.820	-4.840	-4.42	-4.68	-4.56	-4.60	
5978.9300	10.0740	0.004	8.820	-4.840	-4.54	-4.63	-4.48		
6239.6140	12.8390	0.190	—	—		-4.68			
6239.6650	12.8390	0.080	—	—		...			
P II									
4178.4630	9.6350	-0.409	—	—		-6.59	-5.45		
4420.7120	11.0213	-0.33	—	—	-5.16		-5.49	-5.68	NIST
4475.2700	13.0865	0.44	—	—			-5.43	-5.28	NIST
4499.2300	13.3807	0.47	—	—	-4.95		-5.36		NIST
4530.8230	13.0558	-0.56	—	—	-4.43				NIST
4602.0690	12.8532	0.74	—	—	-5.04		-5.37	-5.83	NIST
4943.4970	12.8532	0.06	—	—			-5.24		NIST
4969.7010	12.8124	-0.19	—	—	-4.79	-6.28	-5.25		NIST

Table 9 - continued.

λ (Å)	E_i (eV)	$\log gf$	$\log \gamma_{\text{rad}}$	$\log \gamma_{\text{St}}$	1	2	3	4	Sources
P II									
5296.0770	10.8021	-0.16	—	—	-4.86		-5.09		NIST
5344.7290	10.7367	-0.39	—	—		-6.30	-5.14	-5.60	NIST
5409.7330	10.7549	-0.39	—	—	-4.88		-5.16	-5.36	NIST
5425.8800	10.8021	0.18	—	—	-4.85	-6.29	-5.06		NIST
6034.0400	10.7367	-0.22	—	—			-5.05	-4.77	NIST
6087.8400	10.7549	-0.35	—	—			-5.25		NIST
S II									
3923.4450	16.1980	0.440	9.060	—	-5.75				
4145.0600	15.8670	0.230	8.560	—	-5.41				
4153.0680	15.8990	0.395	8.520	—	-5.56				
4162.6650	15.9440	0.830	8.620	—	-5.88	-5.14	-5.57	-5.64	
4294.4020	16.1350	0.549	8.620	—	-5.85				
4716.2710	13.6170	-0.319	8.880	—	-5.49				
4815.5520	13.6720	0.177	8.870	—		-5.11		-5.26	
4917.1980	14.0030	-0.400	8.760	—			-5.46		
4925.3430	13.5840	-0.235	8.860	—		-5.02	-5.48		
5009.5670	13.6170	-0.094	8.860	—		-5.15			
5014.0420	14.0680	0.030	8.750	—				-5.00	
5032.4340	13.6720	0.282	8.850	—		-5.13	-5.72		
5212.6200	15.0680	0.658	9.190	—		-5.44			
5320.7230	15.0680	0.535	9.090	—		-5.05		-4.96	
5346.0840	15.0680	0.503	9.140	—		-4.73			
5453.8550	13.6720	0.557	8.850	—		-5.06	-5.80		
5473.6140	13.5840	-0.122	8.870	—		-5.04			
5509.7050	13.6170	-0.117	8.880	—		-4.86			
5606.1510	13.7330	0.156	8.180	—		-4.97		-4.82	
5639.9770	14.0680	0.330	8.750	—		-4.97	-5.65		
5640.3460	13.7010	0.147	8.310	—		-5.10	-5.65		
5647.0200	14.0030	0.110	8.750	—		-4.96			
Ca II									
3933.6630	—	0.105	8.207	-6.267	-6.02	-5.28		-5.07	
5019.9710	7.5150	-0.501	7.890	-4.614		-5.48	-5.87		
Sc II									
4314.0830	0.6180	-0.096	8.365	-6.723			-8.68		
4320.7320	0.6050	-0.252	8.364	-6.726			-8.67		
Ti II									
3900.5510	1.1310	-0.280	8.365	-6.674		-5.97			
3913.4680	1.1160	-0.410	8.367	-6.674	-6.46	-5.85	-6.59		
4028.3430	1.8920	-0.990	8.480	-6.566	-6.45	-5.83	-6.52		
4053.8340	1.8930	-1.060	8.384	-6.563	-6.63		-6.64		
4161.5350	1.0840	-2.160	8.471	-6.591		-5.90			
4163.6480	2.5900	-0.210	8.369	-6.625	-6.49	-5.84	-6.58	-6.56	
4287.8720	1.0800	-1.820	8.225	-6.547	-6.59	-5.89	-6.60		
4290.2190	1.1650	-0.930	8.461	-6.665	-6.50				
4294.0990	1.0840	-0.880	8.225	-6.540	-6.59		-6.67		
4300.0490	1.1800	-0.490	8.471	-6.694	-6.45		-6.53		
4301.9140	1.1610	-1.200	8.471	-6.675	-6.55	-5.85	-6.62	-6.59	
4314.9750	1.1610	-1.120	8.479	-6.675			-6.59		
4320.9600	1.1650	-1.900	8.479	-6.665		-5.87			
4367.6590	2.5900	-0.870	8.496	-6.679	-6.56	-5.94	-6.59		
4386.8440	2.5980	-0.940	8.496	-6.680	-6.51	-5.95			
4391.0310	1.2310	-2.240	8.461	-6.542		-5.95			
4394.0510	1.2210	-1.770	8.471	-6.601	-6.51	-5.88	-6.59		
4395.0330	1.0840	-0.510	8.207	-6.505	-6.48		-6.57	-6.62	
4399.7720	1.2370	-1.220	8.461	-6.612	-6.50	-5.83	-6.60	-6.62	
4411.0740	3.0950	-0.670	8.346	-6.537	-6.51	-5.96	-6.57	-6.64	
4417.7190	1.1650	-1.230	8.225	-6.665	-6.52	-5.81	-6.61	-6.53	

Table 9 - continued.

λ (Å)	E_i (eV)	$\log gf$	$\log \gamma_{\text{rad}}$	$\log \gamma_{\text{st}}$	1	2	3	4	Sources
Ti II									
4418.3300	1.2370	-1.990	8.471	-6.601		-5.90			
4421.9380	2.0610	-1.580	8.412	-6.587		-5.97			
4441.7340	1.1800	-2.270	8.225	-6.694		-5.95			
4443.7940	1.0800	-0.700	8.199	-6.509	-6.52	-5.76	-6.59	-6.59	
4450.4820	1.0840	-1.510	8.199	-6.502	-6.58	-5.86	-6.60	-6.52	
4464.4500	1.1610	-1.810	8.217	-6.713	-6.57	-5.86	-6.53		
4468.5070	1.1310	-0.600	8.207	-6.723	-6.53	-5.71	-6.57	-6.30	
4488.3310	3.1240	-0.510	8.342	-6.539	-6.52	-5.93	-6.57		
4501.2730	1.1160	-0.760	8.199	-6.729	-6.52	-5.74	-6.56	-6.64	
4518.3270	1.0800	-2.640	8.431	-6.584		-5.80			
4563.7610	1.2210	-0.790	8.217	-6.713	-6.53		-6.60	-6.74	
4571.9680	1.5720	-0.230	8.367	-6.680	-6.47		-6.57		
4657.2060	1.2430	-2.320	8.207	-6.474		-5.88			
4708.6650	1.2370	-2.370	8.199	-6.729		-5.87			
4763.8810	1.2210	-2.360	8.431	-6.614		-5.91			
4779.9850	2.0480	-1.260	8.262	-6.455	-6.52	-5.86	-6.54		
4798.5210	1.0800	-2.670	8.283	-6.580		-5.88			
4805.0850	2.0610	-0.960	8.262	-6.455	-6.50	-5.82	-6.55	-6.27	
4911.1930	3.1240	-0.650	8.305	-6.533	-6.41	-5.84	-6.49	-6.41	
5069.0900	3.1240	-1.540	8.305	-6.533		-5.99			
5072.2810	3.1240	-0.990	8.369	-6.544		-5.92	-6.59		
5129.1520	1.8920	-1.300	8.365	-6.536	-6.55	-5.81	-6.53		
5154.0700	1.5660	-1.780	8.225	-6.661		-5.81	-6.49		
5185.9130	1.8930	-1.370	8.367	-6.533		-5.83	-6.51		
5188.6870	1.5818	-1.050	8.225	-6.661			-6.60	-6.59	
5211.5360	2.5900	-1.356	8.480	-6.625		-5.98	-6.63		
5226.5430	1.5660	-1.230	8.217	-6.713			-6.58		
5268.6150	2.5980	-1.670	8.384	-6.625		-5.78			
5381.0150	1.5660	-1.970	8.199	-6.729		-5.83			
5418.7510	1.5820	-2.110	8.199	-6.729		-5.83			
Cr I									
4274.7960	—	-0.231	7.380	-6.244		-5.52			
5208.4190	0.9410	0.158	7.716	-6.145		-5.48			
Cr II									
4003.2830	6.4840	-0.601	8.658	-6.620		-5.74	-6.24		
4037.9720	6.4870	-0.557	8.648	-6.621			-6.21	-6.10	
4051.9300	3.1040	-2.360	8.407	-6.716	-6.20			-5.99	
4070.8400	6.4870	-0.751	8.464	-6.621		-5.71	-6.18		
4072.5610	3.7140	-2.460	8.410	-6.653		-5.62	-6.11		
4082.2850	5.3190	-1.234	8.490	-6.615		-6.06			
4132.4190	3.7580	-2.345	8.410	-6.653		-5.71	-6.16		
4145.7810	5.3190	-1.164	8.456	-6.643	-6.15	-5.45	-5.95		
4172.5910	3.1050	-2.356	8.364	-6.718					
4179.4210	3.8270	-1.800	8.410	-6.633	-6.35	-5.66	-6.14		
4224.8600	5.3300	-1.726	8.350	-6.565		-5.02			
4252.6320	3.8580	-1.810	8.410	-6.656	-6.44		-6.17		
4254.5220	5.8710	-0.973	8.431	-6.663		-5.82	-6.25		
4254.5650	8.1840	-1.752	8.443	-6.220		...			
4261.9130	3.8640	-1.340	8.410	-6.656	-6.33				
4269.2770	3.8540	-2.020	8.410	-6.653		-5.62	-6.14		
4275.5670	3.8580	-1.520	8.410	-6.653	-6.40	-5.63	-6.15		
4284.1880	3.8540	-1.670	8.410	-6.649	-6.37		-6.15		
4306.9160	5.8730	-1.185	8.431	-6.661		-5.90	-6.33		
4362.9240	5.6620	-1.887	8.441	-6.613		-5.48			
4539.5950	4.0420	-2.290	8.410	-6.720		-5.51	-5.99	-5.77	
4554.9880	4.0710	-1.282	8.410	-6.639		-5.55		-5.96	

Table 9 - continued.

λ (Å)	E_i (eV)	$\log gf$	$\log \gamma_{\text{rad}}$	$\log \gamma_{\text{St}}$	1	2	3	4	Sources
Cr II									
4558.6500	4.0730	-0.449	8.410	-6.638	-6.19	-5.50			
4565.7400	4.0420	-1.820	8.410	-6.720		-5.56	-6.07		
4588.1990	4.0710	-0.627	8.410	-6.656		-5.43			
4592.0490	4.0740	-1.221	8.410	-6.656	-6.35	-5.59	-6.13	-6.09	
4616.6290	4.0720	-1.361	8.410	-6.653	-6.31	-5.55	-6.09	-5.94	
4618.8030	4.0740	-0.840	8.410	-6.653	-6.30	-5.48	-6.06	-5.82	
4634.0700	4.0720	-0.990	8.410	-6.649	-6.33	-5.51	-6.07	-6.05	
4697.5980	5.6700	-1.880	8.456	-6.643		-5.47			
4812.3370	3.8640	-1.960	8.407	-6.631		-5.58	-6.05		
4824.1270	3.8710	-0.970	8.407	-6.631		-5.38			
4836.2290	3.8580	-1.960	8.407	-6.630		-5.52	-5.98		
4884.6070	3.8580	-2.100	8.407	-6.626		-5.57			
4901.6230	6.4870	-0.826	8.456	-6.792		-5.69	-6.09		
4912.4620	6.4840	-0.948	8.459	-6.648		-5.69	-6.12		
5024.5200	6.2850	-1.541	8.431	-6.652		-5.55			
5153.4990	3.7580	-2.696	8.407	-6.599		-5.20			
5210.8650	3.7580	-2.945	8.420	-6.584		-5.28			
5232.4960	4.0710	-2.093	8.407	-6.639		-5.63	-6.09		
5237.3290	4.0730	-1.160	8.407	-6.638	-6.28	-5.44	-5.98		
5246.7680	3.7140	-2.466	8.364	-6.660		-5.43			
5274.9640	4.0710	-1.290	8.407	-6.639	-6.30		-6.06	-5.86	
5279.8760	4.0730	-2.100	8.407	-6.638	-6.20	-5.39	-5.89		
5280.0540	4.0740	-2.011	8.407	-6.641	-6.17		-6.11		
5308.4250	4.0710	-2.060	8.407	-6.639		-5.36			
5313.5630	4.0740	-1.650	8.407	-6.641	-6.21		-5.95		
5334.8690	4.0720	-1.562	8.407	-6.643	-6.29	-5.56	-6.09	-5.91	
5407.6040	3.8270	-2.151	8.371	-6.654		-5.64	-6.10	-5.83	
5478.3650	4.1780	-1.908	8.407	-6.631		-5.39	-5.86		
5502.0670	4.1680	-1.990	8.407	-6.630		-5.47	-5.95		
5508.6060	4.1560	-2.110	8.407	-6.628		-5.48	-5.91	-5.75	
5620.6310	6.4870	-1.145	8.474	-6.624		-5.63	-6.04		
Mn I									
4030.7530	—	-0.470	7.204	-6.278			-5.29		
4034.4830	—	-0.811	7.149	-6.278		-4.59	-5.23		
4035.7190	2.1430	-0.190	7.953	-6.181		-4.47			
4041.3320	5.0870	-0.032	8.061	-7.701		-4.29			
4041.3550	2.1140	0.285	7.957	-6.174		...	-5.10		
4055.5440	2.1430	-0.070	7.955	-6.182		-4.46	-5.05		
4058.9300	2.1780	-0.446	7.950	-6.177		-4.51		-4.63	
4083.6280	2.1640	-0.250	7.955	-6.182			-4.84		
4278.6730	4.7260	-0.730	7.923	-6.197		-4.26			
4455.0140	3.0720	-0.393	7.957	-5.225		-4.51			
4457.5490	3.0730	-0.117	7.963	-5.217		-4.52			
4458.2540	3.0730	0.042	7.965	-5.134		-4.54			
4461.0790	3.0750	-0.380	7.970	-5.134		-4.38			
4462.0310	3.0750	0.320	7.972	-5.001		-4.51			
4464.6820	2.9200	-0.104	7.848	-4.635		-4.52			
4502.2130	2.9200	-0.345	7.849	-4.112		-4.52			
4727.4610	2.9200	-0.470	7.771	-6.147		-4.33			
4762.3670	2.8880	0.425	7.767	-6.148		-4.43		-4.30	
4765.8460	2.9410	-0.080	7.771	-6.147		-4.37		-4.13	
4766.4180	2.9200	0.100	7.770	-6.147		-4.34		...	
4783.4270	2.2980	0.042	8.004	-5.460		-4.35	-5.02	-4.11	
4823.5240	2.3190	0.144	8.004	-5.460		-4.37	-4.93		

Table 9 - continued.

λ (Å)	E_i (eV)	$\log gf$	$\log \gamma_{\text{rad}}$	$\log \gamma_{\text{St}}$	1	2	3	4	Sources
				Mn II					
3941.2310	5.4370	-1.147	8.348	-6.652					
4081.4440	6.1110	-2.239	8.465	-6.618			-4.65		
4085.0440	5.3730	-2.543	8.420	-6.680			-5.38		
4085.3900	5.5480	-2.561	8.458	-6.661			-5.30		
4085.4050	5.3800	-2.517	8.420	-6.680			...		
4140.4630	5.5670	-2.455	8.489	-6.654		-4.40	-5.22	-4.68	
4171.0330	6.1280	-2.364	8.528	-6.650		-4.14	-4.90		
4171.5120	6.1700	-2.115	8.465	-6.618		-4.39	-5.15		
4180.0640	5.4370	-2.830	8.417	-6.680		-4.56	-5.18		
4184.4540	6.1860	-1.953	8.473	-6.617		-4.44	-5.12		
4200.2700	6.1850	-1.741	8.476	-6.616		-4.37	-5.12		
4201.6310	6.1860	-2.697	8.476	-6.616		-4.60			
4206.3680 ^{hfs}	5.3970	-1.566	8.435	-6.632	-5.81	-4.20	-5.06	-4.30	Holt
4218.3800	6.9130	-1.986	8.348	-6.622		-4.87			
4233.4420	5.8150	-2.675	8.589	-6.582		-4.56	-5.20		
4237.8660	5.3700	-2.959	8.575	-6.621		-4.18	-4.84		
4237.8730	5.3730	-4.124	8.417	-6.628		...			
4240.3900	6.1770	-2.066	8.512	-6.650				-4.20	
4242.9240	5.3730	-2.992	8.575	-6.621			-4.71		
4244.2480	5.3730	-2.396	8.641	-6.614			-4.83		
4245.9220	5.3480	-2.982	8.534	-6.691		-4.87			
4251.7170	6.1850	-1.058	8.528	-6.650	-5.85		-5.12		
4252.9630	6.1860	-1.138	8.512	-6.650	-5.82		-5.05	-4.35	
4253.0250	5.3800	-2.403	8.575	-6.621	...		-5.05	...	
4253.1120	6.1860	-2.092	8.528	-6.650	
4275.8840	7.7580	-1.916	8.553	-6.635		-4.30	-4.89		
4281.9490	5.3730	-2.554	8.620	-6.621	-5.55		-4.85		
4281.9820	10.6500	-0.646	8.227	-4.895		
4283.7690	5.3730	-2.204	8.534	-6.631			-4.75		
4284.4290	5.3700	-2.265	8.442	-6.639			-4.99		
4288.0650	5.3700	-2.756	8.403	-6.641			-4.92	-4.16	
4289.5980	5.3730	-3.306	8.442	-6.639			-4.59		
4293.2660	10.6580	-2.316	8.641	-6.614		-4.75			
4310.6920	10.6700	-0.159	8.237	-5.661		-4.76		-4.57	
4316.8100	5.4370	-3.349	8.486	-6.629			-4.54		
4317.7130	6.9130	-1.917	8.348	-6.621			-5.05		
4363.2550	5.5670	-1.909	8.420	-6.680			-5.31		
4365.2170	6.5730	-1.350	8.464	-6.640			-5.30		
4379.6690	5.4370	-1.850	8.534	-6.631				-4.56	
4393.3790	5.4370	-2.316	8.641	-6.614		-4.75			
4403.5120	6.5730	-1.804	8.473	-6.640			-5.30		
4435.7410	5.4730	-2.580	8.534	-6.631		-4.68	-5.34		
4441.9910	5.4730	-2.355	8.442	-6.639			-5.35	-4.82	
4445.9000	5.4370	-2.856	8.403	-6.641		-4.65			
4478.6370	6.6450	-0.950	8.464	-6.641			-5.27	-4.40	
4496.9860	10.650	-0.861	8.306	-4.688				-4.08	
4497.4630	5.9910	-2.991	8.588	-6.583		-4.77			
4500.5430	5.9930	-2.066	8.588	-6.583		-4.59	-5.34		
4503.2010	5.9910	-2.164	8.589	-6.582		-4.46	-5.22	-4.61	
4518.9560	6.6450	-1.329	8.473	-6.641			-5.28	-4.67	
4639.1520	10.7740	-0.678	8.298	-4.670		-4.74			
4642.6480	9.0070	-2.179	8.699	-6.529		-4.43			
4689.5460	6.1280	-2.535	8.408	-6.602		-4.20			

Table 9 - continued.

λ (Å)	E_i (eV)	$\log gf$	$\log \gamma_{\text{rad}}$	$\log \gamma_{\text{St}}$	1	2	3	4	Sources
Mn II									
4717.2640	6.5360	-1.856	8.684	-6.640		-4.55		-4.62	
4727.4610	2.9200	-2.017	8.415	-6.635				-4.19	
4730.3950	5.3730	-2.147	8.417	-6.634			-4.75	-4.45	
4734.1360	5.3730	-2.879	8.415	-6.635				-4.28	
4770.3510	5.3980	-2.290	8.418	-6.633				-4.23	
4784.6250	6.5730	-1.505	8.684	-6.640		-4.51	-5.28	-4.44	
4791.7820	6.1850	-1.715	8.408	-6.602		-4.55	-5.32	-4.50	
4806.8230	5.4180	-1.559	8.418	-6.633			-5.28		
4830.0610	6.1770	-1.850	8.589	-6.582		-4.38			
4811.6230	5.4180	-2.342	8.417	-6.634			-5.42		
4905.6180	6.5730	-2.271	8.512	-6.650			-5.13		
4998.7560	6.6680	-2.055	8.473	-6.633		-4.62	-5.26		
5029.3760	6.6710	-1.956	8.476	-6.633		-4.56	-5.19		
5049.5280	6.6450	-2.040	8.528	-6.650		-4.49	-5.13		
5067.5430	5.5480	-3.124	8.417	-6.634		-4.66			
5102.0980	5.5670	-3.461	8.418	-6.633				-4.12	
5102.5170	5.9910	-1.934	8.420	-6.608				...	
5103.3170	6.6710	-2.771	8.528	-6.650		-4.16	-4.76		
5107.0920	7.3820	-1.478	8.461	-6.681			-5.03		
5294.3150	9.8620	-0.037	8.895	-5.342			-4.47		
5295.3840	9.8620	0.360	8.893	-5.342			-4.92		
5295.4120	9.8620	0.360	8.893	-5.342			...		
5297.0000	9.8630	-0.214	8.892	-5.342	-6.11		-4.99	-4.08	
5297.0280	9.8630	0.427	8.892	-5.342	
5297.0560	9.8630	0.623	8.891	-5.342	
5299.3020	9.8640	-0.418	8.889	-5.342			-5.15		
5299.3300	9.8640	0.401	8.888	-5.342			...		
5299.3860	9.8640	0.827	8.888	-5.343			...		
5302.3460	9.8650	-0.817	8.884	-5.342			-5.01	-4.27	
5302.4020	9.8650	0.225	8.884	-5.343			
5302.4310	9.8650	0.997	8.884	-5.344			
5331.9640	12.2030	-0.269	8.305	-3.515			-4.58		
5331.9920	12.2030	-0.389	8.305	-3.515			...		
5421.9190	6.1280	-2.184	8.420	-6.680			-4.74	-4.09	
5448.9920	6.1330	-2.374	8.420	-6.680			-4.73		
5501.0830	6.4930	-1.753	8.588	-6.583		-4.56	-5.14		
5556.5170	6.1770	-2.360	8.420	-6.680		-4.34	-5.06		
5559.0470	6.1850	-1.318	8.420	-6.680	-5.73		-4.96	-4.07	
5575.7280	6.1850	-2.501	8.420	-6.680		-4.38			
5578.1260	6.1860	-1.400	8.420	-6.680			-5.00		
5901.6990	6.6710	-1.603	8.408	-6.633		-4.32	-5.18		
5943.8860	6.6580	-2.056	8.589	-6.634		-4.47	-5.10		
6122.4500	10.1840	0.950	9.010	-5.581			-5.30		
6122.8290	10.1840	0.084	9.008	-5.583		-4.47	-5.15		
6125.8610	10.1850	0.783	9.007	-5.573		-4.67			
6126.2250	10.1850	0.230	9.006	-5.575		-4.65			
6128.7330	10.1860	0.588	9.005	-5.576		-4.52	-5.32		
6130.8010	10.1860	0.354	9.003	-5.575			-5.32		
6131.9170	10.1860	0.053	9.003	-5.591		-4.45			
6240.9380	6.8650	-2.092	8.471	-6.563			-4.93		
6370.3080	6.9060	-1.663	8.471	-6.563			-4.96		
Fe I									
3849.9666	1.0110	-0.871	8.223	-6.235	-4.02				
3856.3716	0.0520	-1.286	7.152	-6.324	-4.05				
3872.5012	0.9900	-0.928	8.190	-6.235	-3.96				
3902.9457	1.5570	-0.466	8.167	-6.115	-4.03				
3922.9118	0.0520	-1.651	7.185	-6.324	-4.04				

Table 9 - continued.

λ (Å)	E_i (eV)	$\log gf$	$\log \gamma_{\text{rad}}$	$\log \gamma_{\text{St}}$	1	2	3	4	Sources
Fe I									
3927.9199	0.1100	-1.522	7.152	-6.324	-4.04				
3930.2967	0.0870	-1.491	7.161	-6.324	-4.07				
4005.2420	1.5570	-0.610	8.009	-6.213	-3.99				
4045.8124	1.4850	0.280	8.009	-6.205	-3.95	-4.93	-4.67		
4071.7380	1.6080	-0.022	8.009	-6.212	-4.01	-4.94	-4.66		
4132.0582	1.6080	-0.675	8.013	-6.049	-3.98				
4181.7547	2.8310	-0.371	8.064	-6.159	-3.87				
4191.4307	2.4690	-0.666	8.004	-5.486	-3.91				
4199.0952	3.0470	0.155	7.760	-6.220	-3.88				
4202.0292	1.4850	-0.708	7.905	-6.204		-4.83			
4219.3604	3.5730	—	7.964	-6.209	-3.91				
4227.4266	3.3320	0.266	8.113	-5.272					
4250.1195	2.4690	-0.405	8.009	-5.485	-3.91				
4250.7869	1.5570	-0.714	7.879	-6.204	-3.99				
4260.4670	2.3990	0.109	8.009	-5.486					
4271.7605	1.4850	-0.164	7.940	-6.204	-3.95	-4.93	-4.61	-4.46	
4299.2349	2.4250	-0.405	8.009	-5.486	-3.97				
4325.7619	1.6080	0.006	7.879	-6.203	-4.01				
4383.5450	1.4850	0.200	7.936	-6.204	-3.92	-4.94	-4.62	-4.41	
4404.7504	1.5570	-0.142	7.969	-6.204		-4.89		-4.17	
4415.1225	1.6080	-0.615	7.986	-6.203	-3.94				
4957.5968	2.8080	0.233	8.009	-5.489			-4.45		
5232.9403	2.9400	-0.058	8.009	-5.490				-4.28	
Fe II									
3872.7660	2.7040	-3.316	8.530	-6.588	-4.25				
3898.6020	7.5580	-1.641	8.984	-5.707	-4.11				
3903.7560	7.5390	-1.495	8.989	-5.701		-4.92			
3903.8230	5.5690	-3.501	8.723	-6.580		...			
3906.0350	5.5710	-1.830	8.723	-6.580	-3.87	-4.84			
3908.0720	9.1440	-1.288	9.016	-5.725	-4.01				
3922.0040	9.1260	-1.072	8.985	-5.730	-4.13				
3935.9620	5.5690	-1.860	8.740	-6.566	-3.80	-4.75		-4.35	
3938.2900	1.6710	-3.890	8.462	-6.732	-4.02			-4.65	
3938.9700	5.9110	-1.850	8.613	-6.696	-3.84			-4.50	
3945.2100	1.6950	-4.250	8.462	-6.733	-3.98			-4.46	
3948.7860	7.5390	-2.342	8.990	-5.699	-3.74				
4002.0830	2.7780	-3.472	8.529	-6.590	-4.20			-4.64	
4002.5430	5.9560	-1.709	8.679	-6.695				...	
4012.7440	10.9870	-0.562	8.187	-4.601	-4.19				
4024.5470	4.4950	-2.480	8.489	-6.653	-3.74				
4031.4420	4.7320	-3.115	8.648	-6.614	-3.98		-4.61		
4032.9350	4.4950	-2.703	8.576	-6.664	-3.86				
4041.6410	5.5690	-3.128	8.699	-6.646	-4.00				
4044.0120	4.7320	-2.414	8.699	-6.646			-4.67	-4.50	
4057.4610	7.2740	-1.545	8.581	-6.640	-4.01		-4.63		
4128.7480	2.5830	-3.770	8.614	-6.671	-3.77				
4138.2080	4.7320	-3.177	8.496	-6.678	-4.08				
4138.4050	2.8280	-4.469	8.528	-6.593	-3.83				
4178.8620	2.5830	-2.500	8.491	-6.603	-3.97	-4.97	-4.71		
4199.4910	11.1490	-0.226	8.146	-4.705	-3.65				
4202.5220	6.8070	-2.333	8.682	-6.637	-3.90				
4202.8590	6.8070	-2.613	8.682	-6.637	-3.86				
4205.5950	11.2070	-0.302	8.166	-4.670	-3.69				
4250.4370	7.6840	-1.746	8.947	-5.802	-3.80				
4258.1540	2.7040	-3.400	8.481	-6.599	-4.01	-4.99	-4.73		
4258.3400	2.6420	-4.131	8.612	-6.769	-4.04				
4263.8690	7.6930	-1.712	8.954	-5.802	-3.78		-4.46		
4273.3260	2.7040	-3.258	8.617	-6.674		-4.96	-4.72	-4.58	
4286.2800	7.7080	-1.622	8.961	-5.803	-3.77	-4.73	-4.52	-4.44	
4296.5720	2.7040	-3.010	8.487	-6.602	-3.83	-4.85	-4.60	-4.33	
4303.1760	2.7040	-2.560	8.614	-6.671	-3.87				

Table 9 - continued.

λ (Å)	E_i (eV)	$\log gf$	$\log \gamma_{\text{rad}}$	$\log \gamma_{\text{St}}$	1	2	3	4	Sources
				Fe II					
4319.4130	7.6530	-2.119	9.045	-5.844	-3.88				
4319.6800	7.8450	-1.758	9.009	-5.702	-3.85		-4.48		
4321.3090	7.8690	-1.830	9.026	-5.708	-3.86				
4325.4360	6.1380	-2.337	8.617	-6.580	-3.96				
4325.5400	6.0880	-2.307	8.670	-6.586	...				
4354.3440	7.6530	-1.395	9.042	-5.850	-4.01				
4357.5840	6.0880	-2.113	8.640	-6.582	-3.75		-4.48		
4361.2470	6.1380	-2.114	8.703	-6.580			-4.81		
4369.4110	2.7790	-3.670	8.481	-6.599	-3.88	-4.73	-4.57		
4384.0940	6.2260	-2.280	8.679	-6.564	-4.07				
4384.3190	2.6570	-3.500	8.476	-6.601	-3.97	-4.99	-4.70		
4385.3870	2.7780	-2.680	8.617	-6.674	-3.77				
4413.6010	2.6760	-3.670	8.476	-6.601	-4.34				
4416.8300	2.7780	-2.410	8.614	-6.671	-4.06	-5.11		-4.71	
4431.6050	7.9400	-1.767	9.001	-5.709	-3.88				
4446.2370	5.9560	-2.439	8.723	-6.695	-4.07	-5.08			
4449.6160	7.9290	-1.589	9.010	-5.704	-3.94				
4461.4390	2.5830	-4.114	8.486	-6.585	-4.08				
4461.7060	6.2260	-2.046	8.617	-6.580	-3.88	-4.80	-4.57		
4472.9290	2.8440	-3.430	8.481	-6.599	-3.97		-4.72		
4487.4970	7.6930	-2.141	8.967	-5.866	-3.63				
4489.1830	2.8280	-2.970	8.487	-6.602	-3.87			-4.18	
4491.4050	2.8560	-2.700	8.481	-6.599	-3.93		-4.70	-4.29	
4493.5290	7.9200	-1.427	9.005	-5.702	-3.90		-4.64	-4.24	
4507.1020	7.7730	-1.918	9.024	-5.844	-3.77				
4508.2880	2.8560	-2.250	8.617	-6.674	-3.89	-5.01	-4.72	-4.60	
4515.3390	2.8440	-2.450	8.487	-6.602	-3.89	-4.99		-4.49	
4515.6090	6.2260	-2.736	8.535	-6.581				...	
4520.2240	2.8070	-2.600	8.491	-6.603	-3.90	-4.91		-4.52	
4522.6340	2.8441	-2.169	8.614	-6.671	-3.88			-4.44	
4541.5240	2.8560	-2.790	8.614	-6.671	-4.09	-5.07		-4.72	
4549.1920	5.9110	-1.870	8.699	-6.696		-4.61			
4555.8930	2.8280	-2.160	8.491	-6.603	-4.12			-4.75	
4576.3400	2.8440	-2.920	8.612	-6.668	-3.95	-4.93		-4.60	
4579.5270	6.2260	-2.508	8.640	-6.582	-3.47				
4580.0630	2.5830	-3.725	8.484	-6.588	-4.06				
4582.8350	2.8440	-3.090	8.491	-6.603	-3.99	-4.95		-4.63	
4583.8370	2.8070	-1.860	8.615	-6.666	-3.93			-4.46	
4583.9990	2.7040	-4.216	8.489	-6.583	
4596.0150	6.2260	-1.837	8.744	-6.577	-3.75	-4.76		-4.42	
4598.4940	7.8040	-1.497	9.000	-5.848	-3.85	-4.82	-4.62	-4.54	
4620.5210	2.8280	-3.240	8.615	-6.666		-4.93		-4.37	
4629.3390	2.8070	-2.330	8.476	-6.601	-3.99	-5.02		...	
4635.3160	5.9560	-1.650	8.732	-6.695	-3.60	-4.63		-4.47	
4638.0500	7.7080	-1.518	8.984	-5.859	-3.77	-4.72		-4.36	
4640.8120	7.7080	-1.880	8.980	-5.870	-3.81				
4656.9810	2.8910	-3.610	8.612	-6.668	-3.86				
4666.7580	2.8280	-3.330	8.476	-6.601	-3.88			-4.32	
4731.4530	2.8910	-3.000	8.615	-6.666	-3.94				
4826.6830	10.2880	-0.442	8.948	-5.374	-3.90		-4.53		
4913.2920	10.2880	0.012	8.952	-5.330		-4.83	-4.52	-4.30	
4923.9270	2.8910	-1.320	8.489	-6.583				-3.97	
4948.0960	10.3080	-0.324	8.987	-5.350	-3.79		-4.49		
4948.7930	10.3480	-0.008	9.015	-5.413	-3.81		-4.65		
4951.5840	10.3080	0.175	8.959	-5.268	-3.73		-4.49	-4.30	

Table 9 - continued.

λ (Å)	E_i (eV)	$\log gf$	$\log \gamma_{\text{rad}}$	$\log \gamma_{\text{St}}$	1	2	3	4	Sources
				Fe II					
4953.9870	5.5710	-2.757	8.528	-6.608			-4.57		
4984.4880	10.3290	0.011	9.011	-5.367		-4.81	-4.56	-4.34	
4984.5770	10.4140	-1.257	9.112	-5.424		...			
4990.5090	10.3290	0.177	8.988	-5.350	-3.81		-4.57	-4.32	
4991.4400	10.2730	-0.571	9.100	-5.551			-4.49		
4993.3580	2.8070	-3.640	8.484	-6.588	-3.91		-4.63		
4999.1800	10.2730	-0.483	9.020	-5.895			-4.52		
5001.9590	10.2730	0.896	8.931	-5.326		-4.85	-4.53		
5004.1950	10.2730	0.497	8.932	-5.319		-4.82	-4.56	-4.39	
5006.8410	10.3790	-0.427	8.934	-5.367	-3.68		-4.39		
5007.4470	10.3810	-0.363	8.940	-5.377			-4.55		
5007.7390	10.2880	-0.203	9.035	-4.976	-3.77	-4.77	-4.53		
5018.4400	2.8910	-1.220	8.486	-6.585				-3.99	
5019.4620	5.5690	-2.697	8.543	-6.607			-4.54		
5021.5940	10.2880	-0.300	9.053	-5.189			-4.55		
5022.4200	10.3480	-0.064	9.012	-5.367			-4.63	-4.41	
5022.7920	10.2880	-0.023	9.103	-5.552			-4.53	...	
5026.8060	10.3080	-0.222	9.027	-5.534			-4.58		
5030.6300	10.2880	0.397	9.023	-5.891	-3.78	-4.85	-4.57	-4.51	
5032.7120	10.3910	0.109	8.988	-5.376	-3.83		-4.61		
5035.7080	10.2880	0.606	8.937	-5.320	-3.73	-4.82	-4.55	-4.37	
5036.7180	10.3910	-0.521	9.001	-5.415			-4.55		
5045.1140	10.3080	-0.134	9.052	-4.984			-4.57		
5047.6410	10.3080	-0.068	9.037	-4.976	-3.84				
5048.4350	10.3290	-0.597	9.015	-5.344	-3.85				
5060.2570	10.4480	-0.525	8.932	-5.282	-3.85				
5061.7180	10.3080	0.217	9.055	-5.189			-4.53	-4.43	
5067.8930	10.3290	-0.198	9.057	-5.382	-3.84				
5070.8990	10.3080	0.242	9.024	-5.890	-3.77	-4.87	-4.56	-4.31	
5074.0530	6.8070	-1.973	8.629	-6.605			-4.76		
5075.7640	10.4550	0.277	8.939	-5.282	-3.91	-4.89	-4.66	-4.34	
5081.9010	10.4140	-0.585	9.165	-4.988				-4.40	
5082.2300	10.4140	-0.099	9.004	-5.416				...	
5089.2140	10.3290	-0.035	9.052	-4.984	-3.84		-4.59		
5093.4650	6.8030	-2.140	8.629	-6.618	-3.88			-4.43	
5093.5760	10.3790	0.112	8.973	-5.349	
5093.7800	10.3810	-0.568	9.118	-5.136	-3.82			...	
5097.2710	10.3290	0.308	8.944	-5.269			-4.52		
5100.6070	10.3810	0.171	8.949	-5.270				-4.55	
5100.6640	2.8070	-4.170	8.535	-6.601				...	
5100.7270	10.3810	0.703	8.943	-5.333				...	
5100.8520	5.9110	-1.778	8.699	-6.696				...	
5106.1090	10.3290	-0.276	9.055	-5.189			-4.50		
5115.0620	10.4310	-0.453	9.057	-5.392	-3.87		-4.58		
5117.0340	10.4310	-0.126	9.009	-5.445			-4.58		
5127.8660	5.5710	-2.535	8.529	-6.631			-4.37		
5132.6690	2.8070	-3.980	8.539	-6.599			-4.59		
5144.3550	10.4670	0.283	8.993	-5.397			-4.67		
5146.1270	2.8280	-3.913	8.535	-6.601	-3.99				
5149.4650	10.4480	0.396	8.921	-5.367			-4.54		
5160.8390	5.5690	-2.641	8.528	-6.636			-4.37		
5166.5550	10.4550	-0.030	8.980	-5.377			-4.60		
5169.0330	2.8910	-0.870	8.484	-6.588				-4.25	
5177.0200	10.3790	-0.179	9.014	-5.536	-3.82		-4.54		
5180.3140	10.3910	0.044	9.003	-5.345	-3.85		-4.63		
5197.4800	5.9560	-2.718	8.699	-6.695		-5.00		-4.49	
5197.5770	3.2300	-2.100	8.481	-6.599		
5199.1220	10.3790	0.101	9.024	-4.976			-4.55		
5200.8040	10.3910	-0.371	9.045	-5.383	-3.78		-4.48		
5203.6380	10.3910	-0.046	9.015	-5.536	-3.79		-4.56		

Table 9 - continued.

λ (Å)	E_i (eV)	$\log gf$	$\log \gamma_{\text{rad}}$	$\log \gamma_{\text{St}}$	1	2	3	4	Sources
				Fe II					
5214.4890	10.5030	-0.532	9.006	-5.442	-3.78				
5215.7630	8.1450	-1.522	9.052	-5.822	-3.71				
5215.8440	10.3810	-0.227	9.221	-4.959	...				
5216.8540	10.5030	0.390	8.956	-5.367	-3.80				
5216.8630	10.4800	0.608	8.935	-5.383	...	-4.74			
5224.4110	10.4140	-0.572	9.088	-5.411	-3.80				
5227.1250	6.7030	-2.462	8.547	-6.636	-3.47				
5227.3230	10.5190	-0.026	8.929	-5.392	-3.62				
5227.7590	10.4520	-0.619	8.998	-5.468	-3.81				
5234.6250	3.2210	-2.230	8.487	-6.602	-3.67	-4.79	-4.42		
5243.1920	8.2590	-1.458	8.953	-5.734			-4.45		
5247.9520	10.5310	0.630	8.953	-5.376	-3.98	-5.09		-4.25	
5254.9290	3.2300	-3.227	8.487	-6.602	-3.87		-4.56		
5256.9380	2.8910	-4.250	8.533	-6.602	-3.77				
5257.1220	10.5000	0.032	8.974	-5.408	-3.90				
5260.2590	10.4190	1.069	8.908	-5.365		-4.84			
5270.0270	10.5030	0.068	8.936	-5.375	-4.13				
5272.3970	5.9560	-2.030	8.695	-6.695	-3.64	-4.60	-4.38		
5276.0020	3.1990	-1.940	8.491	-6.603	-3.95	-5.01	-4.65	-4.49	
5278.9380	5.9110	-2.408	8.773	-6.696	-3.89	-4.86	-4.61		
5284.1090	2.8910	-2.990	8.535	-6.601	-3.94		-4.71		
5291.6660	10.4800	0.575	9.000	-5.468	-3.81	-4.91			
5303.3950	8.1850	-1.612	9.025	-5.822			-4.47		
5306.1800	10.5230	0.222	9.063	-5.529	-4.00				
5316.6150	3.1530	-1.850	8.476	-6.601	-3.79				
5316.7840	3.2210	-2.760	8.612	-6.668	-3.74				
5318.7500	10.4190	-0.567	8.917	-5.327	-3.76				
5322.2340	10.4550	-0.518	8.996	-5.346	-3.76				
5325.5530	3.2210	-3.120	8.491	-6.603			-4.62	-4.27	
5339.5850	10.4520	0.537	8.908	-5.436	-3.79				
5346.8560	10.4550	-0.605	9.009	-5.537	-3.73				
5347.1900	10.5600	-0.277	9.048	-5.582	-3.80				
5362.7410	10.5030	-0.402	9.116	-5.133	-3.77				
5362.8690	3.1990	-2.739	8.615	-6.666	...				
5362.9670	10.5000	-0.077	8.904	-5.270	...				
5366.2070	10.5030	-0.270	8.975	-5.342	-3.79				
5375.8470	10.4520	-0.291	9.217	-4.958	-3.66				
5387.0630	10.5220	0.518	8.894	-5.365		-4.85			
5388.0210	10.4520	-0.725	9.010	-5.844	-3.79				
5402.0590	10.5620	0.502	8.912	-5.384		-4.86			
5405.1060	10.5600	-0.268	8.959	-5.445	-3.76				
5414.0730	3.2210	-3.540	8.615	-6.666			-4.63		
5425.2570	3.1990	-3.160	8.476	-6.601	-3.92		-4.61		
5427.8260	6.7240	-1.664	8.540	-6.577			-4.49	-4.16	
5429.9880	10.5960	0.458	8.932	-5.368	-3.83	-4.89			
5534.8470	3.2450	-2.730	8.476	-6.601		-4.91	-4.62		
5534.8900	10.5450	-0.691	8.962	-5.348			
5567.8420	6.7300	-1.887	8.509	-6.578			-4.59		
5643.8800	7.6530	-1.458	8.953	-5.734			-4.55		
5961.7050	10.6780	0.690	9.198	-4.950		-4.98			
6147.7410	3.8890	-2.721	8.530	-6.588			-4.60	-4.11	
6149.2580	3.8890	-2.720	8.530	-6.588			-4.59		
6175.1460	6.2230	-1.983	8.747	-6.632			-4.49		
6238.3920	3.8890	-2.630	8.529	-6.590			-4.58		
6247.3500	6.2090	-2.078	8.609	-6.626				-4.21	
6247.5570	3.8290	-2.310	8.529	-6.590		-4.89		...	
6247.5700	5.9560	-4.011	8.643	-6.695		...			
6305.2960	6.2190	-2.039	8.656	-6.631			-4.53		
6416.9190	3.8920	-2.650	8.528	-6.593			-4.69		
6456.3830	3.9030	-2.100	8.528	-6.593		-4.87	-4.48		

Table 9 - continued.

λ (Å)	E_i (eV)	$\log gf$	$\log \gamma_{\text{rad}}$	$\log \gamma_{\text{St}}$	1	2	3	4	Sources
				Fe III					
4419.5960	8.2410	-2.218	9.061	-6.858	-3.89				
5156.1110	8.6410	-2.018	9.061	-6.858	-3.79				
				Ni II					
3849.5540	4.0320	-1.878	8.741	-6.616			-6.61		
4067.0310	4.0290	-1.835	8.653	-6.617		-6.46	-6.59		
5021.4710	12.4370	0.920	8.944	-5.401				-6.14	
				Sr II					
4077.7090	—	0.167	—	-7.710	-8.35	-8.61	-9.21	-6.00	
				Hg I					
4358.3230	4.8870	-0.383	—	—	-6.58				
5460.7310	5.4610	-0.137	—	—	-6.19	-6.13	-6.36	-4.59	
				Hg II					
3983.9312	4.4030	-1.730	—	—	-6.76	-6.38	-6.75	-5.70	Dolk
5677.1050	13.0858	0.820	—	—	-6.29		-7.02	-5.51	NIST